



Bayesian machine learning framework for characterizing structural dependency, dynamics, and volatility of cryptocurrency market using potential field theory

Anoop C.V., Neeraj Negi, Anup Aprem *

Department of Electronics and Communication Engineering, National Institute of Technology Calicut, Kerala, India

ARTICLE INFO

Keywords:

Cryptocurrency market analysis
Structural dependency
Bayesian data analysis
Potential field method
Gaussian process
Uncertainty characterization

ABSTRACT

Identifying the **structural dependence** between the cryptocurrencies and **predicting market trend** are fundamental for **effective portfolio management** in cryptocurrency trading. In this paper, we present a **unified Bayesian machine learning framework** based on **potential field theory** and **Gaussian Process** to characterize the **structural dependency** of various cryptocurrencies, using **historic price information**. The following are our significant contributions: (i) Proposed a **novel model for cryptocurrency price movements** as a trajectory of a dynamical system governed by a time-varying non-linear potential field. (ii) Developed a Bayesian machine learning framework for **inferring the non-linear potential function from observed cryptocurrency prices**. (iii) Proposed that **attractors and repellers** inferred from the potential field are reliable cryptocurrency market indicators, surpassing existing attributes in the literature. (iv) **Analysis of cryptocurrency market during various Bitcoin crash durations** shows that attractors captured the market trend, volatility, and correlation. In addition, attractors aids explainability and visualization. (v) The **proposed cryptocurrency market indicators (attractors and repellers)** was used to improve the prediction performance of state-of-art deep learning price prediction models.

1. Introduction

Cryptocurrency trading, which has gained enormous popularity in recent years, is viewed as a **high-risk, high-return** investment because of volatility, wherein price fluctuates considerably even within an hour. The volatility of cryptocurrency prices is attributed to many factors such as **unregulated nature of the market, sensitivity to market perception and news, fixed availability of cryptocurrency, and the shift in investor sentiment driven by speculative trading activities by peers**, among others (Cheah & Fry, 2015; Khosravi & Ghazani, 2023). The easiness, of converting from one cryptocurrency to another, offered by cryptocurrency exchanges, and the flexibility for fractional ownership, wherein the investors are allowed to **buy and sell cryptocurrencies in fractional amounts**, facilitating the investment of even small sum of money, are notable advantages of cryptocurrency trading over traditional stock market trading. The crashes of cryptocurrencies, characterized by a cryptocurrency's **price dropping by over 15% within a period of 24 h or longer**, are significant events for cryptocurrency traders (Fruehwirt, Hochfilzer, Weydemann, & Roberts, 2021). By **identifying structural interdependence** between various cryptocurrencies and price change patterns during these crashes, investors can

effectively diversify their portfolios, a well-known strategy in **volatile and uncertain markets** (Peng, Chen, Lin, & Wang, 2024; Zhao, Ma, Li, & Zhang, 2023). In addition, **the structural interdependence between various cryptocurrencies have shown significant changes before and after the occurrences of crash of major cryptocurrencies** such as Bitcoin Fruehwirt et al. (2021).

In addition, experienced and novice investors prefer to use **Automated Financial Consulting (AFC) options for cryptocurrency trading, often called as trading bots or algorithmic trading**, that can automate cryptocurrency portfolio management (Fang et al., 2022; Jing & Kang, 2024; Parente, Rizzuti, & Trerotola, 2024). In the year 2022, **trading bots accounted for more than 60% of all cryptocurrency trading activity** (Balcioğlu & Özer, 2023). Trading bots, typically, use the following strategies (Fang et al., 2022): (i) **continuously track cryptocurrency price movements and dynamically buy, sell, or hold the cryptocurrency to make profits by taking advantage of the volatility of cryptocurrencies**, (ii) **operate in accordance with the hedge investment strategy, maintaining a diversified portfolio by investing in non-correlated cryptocurrencies, to lower the risk associated with an unanticipated crash in price**. These trading bots are implemented using statistical and

* Corresponding author.

E-mail addresses: anoop_p210065ec@nitc.ac.in (Anoop C.V.), neeraj_m210444ec@nitc.ac.in (N. Negi), anup.aprem@nitc.ac.in (A. Aprem).

machine learning (ML) algorithms for risk assessment and portfolio management.

Hence, the requirements of cryptocurrency trading include: (i) the ability to recognize structural dependencies or correlations between individual cryptocurrencies, to do effective portfolio management, (ii) the capability of predicting price patterns (including both rises and falls). However, practical realization of the aforementioned requirements are challenging due to a multitude of reasons, including the following: Though, there exists effective techniques, such as wavelet coherence for inferring structural dependence between the cryptocurrencies, the analysis must be done pairwise, which can be computationally tedious when the number of cryptocurrencies considered are very large. The performance of parametric price prediction models based on price history is poor (accuracy of machine learning based models in predicting cryptocurrency price is less than 65%) (Akyildirim, Goncu, & Sensoy, 2021; Sanders & Saxe, 2017), since they rely on simplistic features such as mean, starting, or closing prices to quantify market trends, which may not be reliable due to the high volatility of cryptocurrency markets, especially during crash periods.

Further, since, a large fraction of cryptocurrency market investors are novices in cryptocurrency trading, market psychology plays a predominant role in the dynamics of cryptocurrency market, wherein the trading activities of the investors are driven by the market sentiments. Market psychology, in turn is very difficult to quantify, and is influenced by multitude of intrinsic and extrinsic factors (Khedr, Arif, El-Bannany, Alhashmi, & Sreedharan, 2021). Hence, approaches, that uses traditional market fundamentals such as supply, demand, cost of production and number of competitors, fail to model the cryptocurrency price evolution accurately. We address these gaps by developing a unified Bayesian machine learning framework that infers market trends, volatility and structural dependencies using a more intuitive and comprehensive approach, by learning a latent potential field that characterizes the collective effects of multiple factors influencing cryptocurrency prices, without explicitly observing individual factors. Our potential field characterization captures the structural dependence between cryptocurrencies without relying on pairwise analysis, aids in visualization and an intuitive understanding of cryptocurrency price evolution and volatility.

In this context, the following are the significant contributions of this paper:

1. Proposed a novel model where the price movements of the cryptocurrencies are governed by a time-varying non-linear potential field function. The potential field theory treats the price of various cryptocurrencies as a trajectory of a chaotic dynamical system.
2. Developed a Bayesian machine learning framework for inferring the non-linear potential function from the observed cryptocurrency prices.
3. The framework of potential field theory lends itself to the notion of attractors and repellers, the states, towards which a dynamical system will eventually converge, and, away from which the time series will diverge, respectively. We propose that attractors and repellers are more reliable cryptocurrency market indicators than existing attributes in the literature such as open, close, or mean prices. Further, the attractors and repellers of the inferred potential field yield better performance when used as a feature for price prediction in existing deep learning models and machine learning models. We conducted an ablation study to assess the impact of our proposed feature, the mean attractor, on cryptocurrency price forecasting models. Specifically, we evaluated its effect on a hybrid LSTM model and other popular architectures used for cryptocurrency price prediction (Tanwar et al., 2021). Our results show that incorporating the mean attractor feature improves the performance of deep learning cryptocurrency price prediction models up to a 24 day horizon.

4. Analysis of the cryptocurrency market data during different Bitcoin crash durations, from April 2017 to November 2021, showed that attractors or repellers captured the market trend and volatility. In addition, such a characterization aids explainability and visualization through: (i) inferring the direction of cryptocurrency price correction and the corresponding confidence level, (ii) characterizing the volatility and correlation of cryptocurrency prices, (iii) inferring the direction of asset movement in cryptocurrency market, (iv) analysis of convergence characteristics of the market, (v) predicting the temporal evolution of the market trends.
5. The structural dependence, inferred using the proposed approach, is compared with the results obtained using the widely used wavelet coherence approach in Fruehwirt et al. (2021), Qiao, Zhu, and Hau (2020) and results obtained were found to be consistent. However, unlike wavelet coherence analysis, the proposed approach can be readily generalized for more than 2 cryptocurrencies.

The paper is structured as follows: Section 2 provides an overview of the relevant literature. The theoretical aspects of the proposed methodology are discussed in Section 3. Section 3.1, proposes the non-linear potential function model, and, establishes the existence of a valid potential function, using Lyapunov stability analysis. Section 3.2 defines attractors and repellers of the potential field using the canonical vector calculus operations. Section 3.3 presents the theoretical aspects of the Bayesian framework for inferring the potential field. Section 3.4 elaborates on the probabilistic approach for inferring attractors and repellers. Section 3 finally summarizes the proposed methodology with the help of a model framework diagram. The numerical results are presented in detail in Section 4. Section 4.1 describes the cryptocurrency datasets and the various Bitcoin crash durations, that this paper focuses on. Section 4.2 presents the numerical results and inferences drawn from Lyapunov stability analysis. Section 4.3 explains the numerical results and insights of cryptocurrency market analysis of two cryptocurrencies (Bitcoin and Ethereum) during the various Bitcoin crash durations. Section 4.4 extends the market analysis results to top 10 cryptocurrencies. Section 4.5 examines the consistency between the proposed potential field approach and the results obtained from the wavelet coherence approach in characterizing structural dependencies. Section 4.6 discusses the performance improvement in price prediction of existing deep learning models when the inferred mean attractor is used as one of the input features. Section 4.7 presents an ablation study, using a diverse set of machine learning and deep learning models commonly used in cryptocurrency price prediction, to rigorously assess the effectiveness of mean attractor as an indicator of market trend and structural dependence. Finally Section 5 offers concluding remarks.

2. Literature review

The majority of the investors in cryptocurrency market are lay investors, with none or limited prior experience in cryptocurrency trading. The phenomena of market psychology and peer influence are more predominant in cryptocurrency market than conventional stock markets (Fruehwirt et al., 2021). Dynamics of collective behaviour of the agents in a multiple agent system, such as cryptocurrency market, is often non-linear in nature and difficult to characterize (de Miranda Cardoso, Ying, & Palomar, 2021; Fei, Shi, & Lim, 2023; Rubio Scola, Garcia Carrillo, & Hespanha, 2023). Given the significant differences between the conventional stock market and the cryptocurrency market, the tools, and approaches that were developed and deployed for the 'conventional' stock market cannot be readily applied for the cryptocurrency market (Herzen et al., 2022; Khedr et al., 2021; Kumbure, Lohrmann, Luukka, & Porras, 2022; Phillips & Gorse, 2018). In addition, cryptocurrency trading bots (Khurana, Singh, & Garg, 2023; Kumlungmak & Vateekul, 2023; Majidi, Shamsi, & Marvasti, 2024; Srinivas Murthy, Akshay, & Hanji, 2022), are preferred

by novice and experienced traders to automate the cryptocurrency exchange and portfolio management. Inferring the structural dependence between the cryptocurrencies, and predicting their price movement, are two important aspects that facilitate efficient cryptocurrency portfolio management (Chuen, Guo, & Wang, 2017).

2.1. Correlation and structural dependency of cryptocurrencies

Identifying structural relations between entities have become an increasingly popular research direction in the field of AI (Ji, Pan, Cambria, Marttinen, & Yu, 2022). A plethora of literature exists on the topic of structural dependence between various cryptocurrencies, with wavelet coherence approach (Fruehwirt et al., 2021; Phillips & Gorse, 2018; Qiao et al., 2020), emerging as the widely used statistical approach, because of its ability to handle non stationarity of cryptocurrency market as well as in capturing both long term and short term dependencies. Generalized Autoregressive Conditional Heteroscedasticity (GARCH) (Antonakakis, Chatzantoniu, & Gabauer, 2019; Aras, 2021; Gao, He, & Kuruoglu, 2021; Jiang, Zhou, & Qiu, 2023), which is mainly used to infer the volatility of returns, is also capable of characterizing structural dependence between cryptocurrencies (Jiang et al., 2023). Time Lagged Cross Correlation (TLCC) (Vassiliadis, Papadopoulos, Rangoussi, Konieczny, & Gralewski, 2017) and entropy based measures (Almeida, Dionísio, Vieira, & Ferreira, 2023) are some alternative methods for finding correlation between cryptocurrencies. However, the correlation analysis using all these approaches, have a common limitation of having to consider distinct pairwise combinations of cryptocurrencies, which is not a scalable approach as the number of cryptocurrencies is high as 1800 (as of March 2022) (Alatorre, Gershenson, & Mateos, 2023).

2.2. Prediction of cryptocurrency prices:

Another line of work uses statistical, and ML based techniques for prediction of price movements or volatility in cryptocurrency market. The two commonly used metrics used to evaluate performance of price prediction models are: Mean Absolute Error (MAE) and Mean Squared Error (MSE). MAE captures the average performance of a price predictive model (Willmott & Matsuura, 2005), whereas, MSE represents the ability of the model in capturing extreme events such as crash (Chai & Draxler, 2014). Compared to classical machine learning models such as linear regression, quadratic discriminant analysis and support vector machines, recurrent neural networks were found to be performing better, in terms of MSE and MAE, because of its ability to capture long term dependencies (Mudassir, Bennbaia, Unal, & Hammoudeh, 2020; Sezer, Gudelek, & Ozbayoglu, 2020; Shen, Wan, & Leatham, 2021). Similarly, RNN based techniques were found to perform better compared to statistical econometric models such as GARCH. Within RNN based techniques, Long Short Term Memory (LSTM) (Gajamannage, Park, & Jayathilake, 2023; Khedr et al., 2021; Tanwar et al., 2021) is the most popular model for cryptocurrency price prediction — refer to recent survey in Murray, Rossi, Carraro, and Visentin (2023) for a comparative study between various models. However, the error performance of models, that predict the cryptocurrency price, solely based on historic prices, has enormous scope for improvement, especially in capturing extreme events like cryptocurrency crashes (Murray et al., 2023).

2.3. Input features of the cryptocurrency price prediction models

Various models, in literature, available for cryptocurrency price prediction, differs from one another mainly in terms of the input features used. The factors that influence the cryptocurrency price can be either internal or external factors (Khedr et al., 2021). Internal factors include technology related aspects of cryptocurrency, such as, coin circulation, reward system and mining difficulty, and are mostly deterministic. The external factors include various sub-factors, that

reflect the market demand and investor sentiment, such as popularity of a cryptocurrency, speculations about market, gold price, restrictions imposed by government, legalizations, Google Trend (Hassani, Huang, & Silva, 2018) and, volume and sentiments of tweets in Twitter (Abraham, Higdon, Nelson, & Ibarra, 2018; Critien, Gatt, & Ellul, 2022), among others (Khosravi & Ghazani, 2023; Zhou, Song, Xiao, & Ren, 2023). Since market psychology and peer influence play an important role in the dynamics of cryptocurrency market, the factors driving cryptocurrency price change from time to time, making it challenging to construct a reliable and sustainable predictive model. In their respective works, Chuen et al. (2017) and Khedr et al. (2021) evaluated the performance of various cryptocurrency price prediction models based on the choice of input features. They concluded that incorporating a combination of time series of historical prices and other internal and external factors that influence cryptocurrency prices as input features can enhance the performance of predictive models, compared to models based solely on any one of these features.

2.4. Use of structural dependence information in cryptocurrency price prediction models:

There are recent attempts to supplement the ML models with structural dependency model to further improve the accuracy of cryptocurrency price prediction. Zhong et al. (2023) uses the correlation metric obtained using Graph Attention Network (GAT) to serve as an additional input feature to an LSTM based predictive model, while, Tanwar et al. (2021), presented a hybrid approach, that exploits the structural dependence between LTC and BTC, to further improve the performance of LSTM based approaches, in LTC price prediction. Tanwar et al. (2021) used time series of opening and mean prices of hourly windows to make predictions over, 1, 3, 7 and 30 days. In addition to the historic prices of LTC (referred as child coin), the direction of price movement of BTC (referred as parent coin) within 1-hour windows was also used as an input feature to the model in Tanwar et al. (2021). However, the opening and mean price need not necessarily represent the exact market trend or dynamics and structural dependence during the observation window, since the cryptocurrency prices are highly volatile, and hence may affect the reliability of the predictions made. Further, given a finite length time series of cryptocurrency price observation, the question, ‘which attributes of the cryptocurrency time series will reliably represent the market dynamics and the volatility characteristics?’, is still an open research problem.

This motivates the need for a unified framework, that can reliably quantify the market trend and underlying uncertainty, while characterizing the structural dependence between various cryptocurrencies, given any time series of cryptocurrency price observations.

3. Proposed methodology: The potential field approach

The proposed approach, in this paper, models the dynamics of the cryptocurrency market using a time-varying potential function over an M -dimensional state space of prices. The cryptocurrency price, at each time, can be considered to be analogous to the position of a hypothetical particle of unit mass on a space-time surface, governed by a gravitational potential field. A particle in a potential field tends to move towards its minima, defined as attractors or sink, and away from its maxima, defined as repeller or source.

Sections 3.1 and 3.2 define the potential field model, considered in this paper, and establishes existence of a potential field in the cryptocurrency market, through Lyapunov stability analysis from non-linear dynamical systems. In Section 3.3, we consider the problem of inference of the potential field using Bayesian machine learning, specifically using Gaussian processes. In Section 3.4, we consider the problem of identifying significant attractors and repellers of the potential field, which we postulate as characterizing the structural dependency of the cryptocurrency market and providing information about the market trend.

3.1. Potential field model for the cryptocurrency market: Lyapunov stability analysis

The time evolution of a hypothetical unit mass, in general, can be described by the following set of nonlinear differential equations

$$\dot{\mathbf{x}} = \frac{d\mathbf{x}}{dt} = f(\mathbf{x}, t), \quad (1)$$

where, $\mathbf{x} \in \mathbb{R}^M$ is a state space vector, and the vector function $f(\cdot)$ determines the system's evolution over time. A potential field, if it exists, $\phi(\cdot)$, is a function whose gradient, $\nabla\phi(\cdot)$, gives the force acting on the particle, where, ∇ , is the spatial derivative operator. A valid potential function, $\phi(t, \mathbf{x})$, if it exists, is related to the vector function $f(\mathbf{x}, t)$ as

$$-\nabla\phi(t, \mathbf{x}) = \frac{df(\mathbf{x}, t)}{dt} = \frac{d^2\mathbf{x}}{dt^2}, \quad (2)$$

i.e. the negative of the spatial derivative (gradient) of a potential function is the same as the time derivative of $f(\cdot)$ at a given time.

Let M and N denote the total number of cryptocurrencies and the total number of price observations, respectively. At a given time¹ t_n , $n = 1, 2, \dots, N$, the vector of prices of all cryptocurrencies (position vector of unit mass) can be denoted as $\mathbf{x}_n = [x_{1,n}, x_{2,n}, \dots, x_{M,n}]^T$. The sequential solution of (1), starting from an initial state, \mathbf{x}_1 , forms a trajectory, denoted by $\zeta_{1:N} = \{\mathbf{x}_1, \dots, \mathbf{x}_N\}$.

The existence of a non-linear potential function, as in (2) is given by the following theorem (Yuan, Ma, Yuan, & Ao, 2013):

Theorem 3.1. For a certain dynamical system, (i) explicit formulation of a function of the form (1) can be given for any global Lyapunov function of the system, (ii) any potential function ϕ obtained from (2) is a global Lyapunov function, and (iii) if a trajectory belongs to a stable dynamic system in the Lyapunov sense, it is equivalent to the existence of a non-linear potential function, with a stable state, defined in its state space.

The proof of Theorem 3.1, available in Yuan et al. (2013) and Ma, Tan, Yuan, Yuan, and Ao (2014), is derived from the notion of conservation of total energy, of the system given by (1).

A system is said to be *stable* in the Lyapunov sense, if the separation between two trajectories of the system with nearby² initial states converge to a single point, namely the attractor. If two nearby trajectories diverge away as time evolves, the system is said to be *unstable*. Lyapunov Stability analysis (Biswal & Dasgupta, 2002; Meng, Shi, Zhang, Bai, & Lin, 2022; Vulpiani, Cecconi, & Cencini, 2009) is a technique from chaos theory (Cambel, 1993) to determine the stability of the non-linear dynamic system in (1). Let $\delta_x(t)$ be the difference vector at time t between two nearby trajectories that start at \mathbf{x}_i and $\mathbf{x}_i + \delta_x(i)$, respectively. The average exponential rate of growth or decay of the norm, $|\delta_x(t)|$ over time, is given by:

$$|\delta_x(t)| = \exp(\lambda t) |\delta_x(i)|, \quad (3)$$

where, λ is the Lyapunov exponent, and is defined as

$$\lambda = \lim_{t \rightarrow \infty} \left[\frac{1}{t} \log \frac{|\delta_x(t)|}{|\delta_x(i)|} \right]. \quad (4)$$

i.e., we can compute the Lyapunov exponents by comparing the time evolution of a perturbed trajectory with the original trajectory, that starts at some point \mathbf{x}_i .

If we do not have the functional form of $f(\mathbf{x}, t)$ and only a sample trajectory is available, we can apply Algorithm 1, described in Rosenstein, Collins, and De Luca (1993), to estimate the Lyapunov exponents

¹ In this paper, we assume that time is discretized, with some sampling interval Δt .

² Two states in a state space are said to be nearby, if the separation between them is less than a small positive quantity, ϵ .

from the given trajectory. Algorithm 1 takes $\zeta_{1:N}$ as input and generates a list of Lyapunov exponents, L . It proceeds by identifying all possible pairs of points \mathbf{x}_i and \mathbf{x}_j , in the trajectory, such that $i < j$ and $i < (N - k)$, where k is a small positive integer that denotes the sampling interval in terms of number of samples. Further, it determines the distance between the subsequent points that are integer multiples of k time steps ahead, starting at all \mathbf{x}_i and \mathbf{x}_j , in order to calculate the exponent estimates in Eq. (4).

Algorithm 1 Finding Lyapunov Exponents from Trajectory (Rosenstein et al., 1993)

```
Require:  $\zeta_{1:N} = \{\mathbf{x}_i\}_{i=1}^N, \epsilon, k, \Delta t$ 
1:  $i \leftarrow 1, L \leftarrow \{\}$ 
2: while  $i \leq N - k$  do
3:    $j \leftarrow i + 1$ 
4:   while  $j \leq N$  do
5:     if  $\|\mathbf{x}_i - \mathbf{x}_j\| \leq \epsilon$  then
6:        $p \leftarrow 1, N_{ij} \leftarrow \lfloor (N - j) / k \rfloor, \lambda_{ij} \leftarrow 0$ 
7:       while  $p \leq N_{ij}$  do
8:          $\lambda_p \leftarrow \left[ \frac{1}{pk\Delta t} \right] \log \left[ \frac{\|\mathbf{x}_{i+kp} - \mathbf{x}_{j+kp}\|}{\|\mathbf{x}_i - \mathbf{x}_j\|} \right]$ 
9:          $\lambda_{ij} \leftarrow \lambda_{ij} + \lambda_p$ 
10:         $p \leftarrow p + 1$ 
11:      end while
12:      end if
13:       $L \leftarrow \{L, \frac{\lambda_{ij}}{N_{ij}}\}, j \leftarrow j + 1$ 
14:    end while
15:     $i \leftarrow i + 1$ 
16:  end while
17: Output:  $L$ 
```

The largest Lyapunov exponent, $\lambda_1 = \max(L)$, determines the rate of divergence or convergence of nearby trajectories in state space. If λ_1 is negative, then nearby trajectories converge towards the attractor³. Conversely, if λ_1 is positive, then nearby trajectories diverge away, indicating the system is unstable. Since Lyapunov stability imply the existence of a valid potential function according to Theorem 3.1, if the trajectory belongs to a Lyapunov stable system, the attractor inferred from the trajectory, will be a stable state towards which the market tends to stabilize during the observation window.

3.2. Laplacian of a scalar potential field and the attractor

This section defines the concepts of attractors and repellers of a potential field with the help of canonical vector calculus operations on the potential gradient. The potential gradient, $\nabla\phi$, in (2), at $\mathbf{x} = [x_1, x_2, \dots, x_N]^T$, at any given time, t , can be represented as a vector in (5)

$$\nabla\phi = \left[\frac{\partial\phi}{\partial x_1}, \frac{\partial\phi}{\partial x_2}, \dots, \frac{\partial\phi}{\partial x_M} \right]^T, \quad (5)$$

where, the time and state arguments of the potential functions are suppressed for the convenience of representation. The negative of the gradient vector, $-\nabla\phi$, is a vector field, normally visualized as lines of flux, represents the amount of acceleration and the direction of the evolution, of the state, under the influence of the potential field. The, divergence, of any vector field \mathbf{F} , denoted by $\nabla \cdot \mathbf{F}$, represents the density of a vector field's outward flux from an infinitesimally small volume surrounding a certain point. The Laplacian of a scalar potential function (ϕ) is the divergence of the potential gradient, that quantifies the net

³ An attractor is a set of points in state space towards which a system evolves over time. More specifically, an attractor is a subset of the state space that is invariant under the dynamics of the system, meaning that once a trajectory enters the attractor, it stays there indefinitely or until it is perturbed by some external influence (Cambel, 1993).

out-flux from an infinitesimal hypercube centred at a point in the state space, and can be evaluated as in (6):

$$\nabla^2\phi = \nabla \cdot \nabla\phi = \sum_{i=1}^M \frac{\partial^2\phi}{\partial x_i^2}. \quad (6)$$

When the Laplacian of the potential field, at a particular point in the state space, is positive it signifies that the net out-flux, in that region, is positive. This, in turn, indicates that the net force exerted on the particle will be oriented outward, propelling the particle away from that region – such regions are classified as repellers or sources. Conversely, if the Laplacian is negative, it denotes that the net force acting on a particle will be directed inward, leading to the stabilization of the particle in that region – such regions are referred to as attractors or sinks. Hence, the attractors and repellers can be estimated as the regions in the state space with negative and positive Laplacian values, respectively.

The Bayesian approach adopted for inferring the potential function and the attractors and repellers of the potential function from the observed trajectory is discussed in Section 3.3.

3.3. Bayesian approach for inferring the potential function

The trajectory $\zeta_{1:N}$ gives noisy observations of f as in (1), which, in turn, can be used to estimate the potential gradient $\nabla\phi$ using (2). Let,

$$\mathbf{y}_i = \nabla\phi(\mathbf{x}_i) + \eta, \quad \eta \sim \mathcal{N}(0, \sigma^2), \quad (7)$$

where, $\nabla\phi$ is the gradient of unknown potential function, which maps any state \mathbf{x} to the corresponding potential gradient at \mathbf{x} , and the noise term η characterize the randomness in the price observation as well as that incurred in the estimation of the gradient.

We model, $\nabla\phi$, as a multi-input multi-output Gaussian Process (GP) (Berkenkamp, Schoellig, & Krause, 2019; Letham & Bakshy, 2019; Roberts et al., 2013; Schulz, Speekenbrink, & Krause, 2018), which is a distribution over functions, as

$$\nabla\phi(\mathbf{x}) \sim GP(\mu(\mathbf{x}), k(\mathbf{x}, \mathbf{x}')), \quad (8)$$

where, $\mu(\mathbf{x}) = \mathbb{E}(\nabla\phi(\mathbf{x}))$, is the mean function, and $k(\mathbf{x}, \mathbf{x}')$ is the covariance function. In our work, $\mu(\mathbf{x})$ is set to zero. The covariance function $k(\mathbf{x}, \mathbf{x}')$, also known as the GP kernel, characterizes the similarity between the values of the function at any two distinct input states, \mathbf{x} and \mathbf{x}' , and is defined as

$$k(\mathbf{x}, \mathbf{x}') = \mathbb{E}[(\nabla\phi(\mathbf{x}) - \mu(\mathbf{x}))^T (\nabla\phi(\mathbf{x}') - \mu(\mathbf{x}'))]. \quad (9)$$

In practice, the function k is chosen based on the anticipated nature of the function to be inferred. In our context, we use a squared exponential (SE) kernel, under the assumption of a smooth infinitely differentiable potential function (Lahmiri, Bekiros, & Bezzina, 2022; Tran, Rossi, Milios, & Filippone, 2022; Williams & Rasmussen, 2006). The extension to other GP kernels is straightforward. The SE kernel is given by

$$k_{SE}(\mathbf{x}, \mathbf{x}') = \sigma_{SE}^2 \exp\left(-\frac{1}{2}(\mathbf{x} - \mathbf{x}')^T \Lambda^{-1}(\mathbf{x} - \mathbf{x}')\right), \quad (10)$$

where, $\Lambda = \text{diag}(\lambda_1, \dots, \lambda_M) \in \mathbb{R}^{M \times M}$ is a diagonal matrix of input scale length hyperparameters $\{\lambda_i\}_{i=1}^M$ and σ_{SE} is the signal variance hyperparameter.

Let $\mathbf{X}_\zeta = [\mathbf{x}_1^T, \dots, \mathbf{x}_N^T]^T$ be a matrix, with each row representing the transpose of the state vector in the trajectory, and $\mathbf{Y}_\zeta = [\mathbf{y}_1^T, \dots, \mathbf{y}_N^T]^T$, the matrix of noisy observations of potential gradients. Given a set of Q new states (test points) in the state space, represented as a matrix $\mathbf{X}^* = [\mathbf{x}^{*T}_1, \dots, \mathbf{x}^{*T}_Q]^T$, we can infer the corresponding potential gradient by computing the posterior distribution, $p(\nabla\phi(\mathbf{X}^*) | D_\zeta)$. By definition of GP, $\mathbf{Y}_\zeta \in \mathbb{R}^{N \times M}$ and $\nabla\phi(\mathbf{X}^*) \in \mathbb{R}^{Q \times M}$ are jointly distributed as

$$\begin{bmatrix} \mathbf{Y}_\zeta \\ \nabla\phi(\mathbf{X}^*) \end{bmatrix} = \mathcal{N}\left(0, \begin{bmatrix} \mathbf{K}(\mathbf{X}_\zeta, \mathbf{X}_\zeta) + \sigma^2 \mathbf{I} & \mathbf{K}(\mathbf{X}_\zeta, \mathbf{X}^*) \\ \mathbf{K}(\mathbf{X}^*, \mathbf{X}_\zeta) & \mathbf{K}(\mathbf{X}^*, \mathbf{X}^*) \end{bmatrix}\right), \quad (11)$$

where, $\mathbf{K}(\mathbf{X}_\zeta, \mathbf{X}_\zeta) \in \mathbb{R}^{N \times N}$ is the covariance matrix between the training points, $\mathbf{K}(\mathbf{X}_\zeta, \mathbf{X}^*) \in \mathbb{R}^{N \times Q}$ is the covariance matrix between all past observations and all test points, $\mathbf{K}(\mathbf{X}^*, \mathbf{X}_\zeta) \in \mathbb{R}^{Q \times N}$ is the covariance matrix between all the test points and the training, $\mathbf{K}(\mathbf{X}^*, \mathbf{X}^*) \in \mathbb{R}^{Q \times Q}$ is the covariance matrix between all test points, σ^2 is the variance of η and $\mathbf{I} \in \mathbb{R}^{N \times N}$ is an identity matrix. The posterior mean and variance of $\nabla\phi(\mathbf{X}^*)$ can be computed as (12) and (13), respectively.

$$\mathbb{E}[\nabla\phi(\mathbf{X}^*)] = \mathbf{K}(\mathbf{X}_\zeta, \mathbf{X}^*)^T (\mathbf{K}(\mathbf{X}_\zeta, \mathbf{X}_\zeta) + \sigma^2 \mathbf{I})^{-1} \mathbf{Y}_\zeta, \quad (12)$$

$$\text{Var}[\nabla\phi(\mathbf{X}^*)] = \mathbf{K}(\mathbf{X}_\zeta, \mathbf{X}^*) - \mathbf{K}(\mathbf{X}_\zeta, \mathbf{X}^*)^T (\mathbf{K}(\mathbf{X}_\zeta, \mathbf{X}_\zeta) + \sigma^2 \mathbf{I})^{-1} \mathbf{K}(\mathbf{X}_\zeta, \mathbf{X}^*). \quad (13)$$

Assuming $\nabla\phi$ at any given state is given by (5), its Jacobian matrix can be expressed as

$$J(\nabla\phi) = \frac{\partial \nabla\phi}{\partial \mathbf{x}^*} = \begin{bmatrix} \frac{\partial^2\phi}{\partial x_1^2} & \frac{\partial^2\phi}{\partial x_1 \partial x_2} & \dots & \frac{\partial^2\phi}{\partial x_1 \partial x_M} \\ \frac{\partial^2\phi}{\partial x_2 \partial x_1} & \frac{\partial^2\phi}{\partial x_2^2} & \dots & \frac{\partial^2\phi}{\partial x_2 \partial x_M} \\ \vdots & \vdots & \ddots & \vdots \\ \frac{\partial^2\phi}{\partial x_M \partial x_1} & \frac{\partial^2\phi}{\partial x_M \partial x_2} & \dots & \frac{\partial^2\phi}{\partial x_M^2} \end{bmatrix}. \quad (14)$$

Since the derivative operation is an affine transformation, and an affine transformation of a GP is again a GP, the individual elements of the Jacobian Matrix in (14), at each test state \mathbf{x}^* , can be inferred from the derivative of the GP that models $\nabla\phi$. The squared exponential kernel for the first and second order derivatives, respectively, of the GP in (8), are given by (15) and (16).

$$\frac{\partial \mathbf{k}(\mathbf{x}^*, \mathbf{x})}{\partial \mathbf{x}^*} = \Lambda^{-1}(\mathbf{x}^* - \mathbf{x}) \mathbf{k}(\mathbf{x}^*, \mathbf{x}) \in \mathbb{R}^M. \quad (15)$$

$$\frac{\partial^2 \mathbf{k}(\mathbf{x}^*, \mathbf{x})}{\partial \mathbf{x}^* \partial \mathbf{x}^*} = \Lambda^{-1}((\mathbf{x}^* - \mathbf{x})(\mathbf{x}^* - \mathbf{x})^T \Lambda^{-1} - \mathbf{I}) \mathbf{k}(\mathbf{x}^*, \mathbf{x}). \quad (16)$$

In (15) and (16), \mathbf{x}^* and \mathbf{x} are test and train input states, respectively. The posterior mean, and the associated covariance of $J(\nabla\phi)$, at a test input \mathbf{x}^* , can be computed as (17) and (18).

$$\mathbb{E}\left[\frac{\partial \nabla\phi(\mathbf{x}^*)}{\partial \mathbf{x}^*}\right] = \frac{\partial \mathbf{K}(\mathbf{X}_\zeta, \mathbf{x}^*)^T}{\partial \mathbf{x}^*} (\mathbf{K}(\mathbf{X}_\zeta, \mathbf{X}_\zeta) + \sigma^2 \mathbf{I})^{-1} \mathbf{Y}_\zeta, \quad (17)$$

$$\text{Var}\left[\frac{\partial \nabla\phi(\mathbf{x}^*)}{\partial \mathbf{x}^*}\right] = \frac{\partial^2 \mathbf{K}(\mathbf{x}^*, \mathbf{x}^*)}{\partial \mathbf{x}^* \partial \mathbf{x}^*} - \frac{\partial \mathbf{K}(\mathbf{X}_\zeta, \mathbf{x}^*)^T}{\partial \mathbf{x}^*} (\mathbf{K}(\mathbf{X}_\zeta, \mathbf{X}_\zeta) + \sigma^2 \mathbf{I})^{-1} \frac{\partial \mathbf{K}(\mathbf{X}_\zeta, \mathbf{x}^*)}{\partial \mathbf{x}^*}, \quad (18)$$

where $\frac{\partial \mathbf{K}(\mathbf{X}_\zeta, \mathbf{x}^*)}{\partial \mathbf{x}^*}$ in (17), is the derivative covariance matrix between all input training points, \mathbf{X}_ζ and the test point, \mathbf{x}^* , computed using the derivative kernel in (15). Similarly, $\frac{\partial^2 \mathbf{K}(\mathbf{x}^*, \mathbf{x}^*)}{\partial \mathbf{x}^* \partial \mathbf{x}^*}$ is the derivative covariance, between the test input \mathbf{x}^* and itself, computed using (16). (17) and (18) gives the posterior inferences about all the elements in (14). Since, the Laplacian in (6) is the trace of the Jacobian matrix in (14), the posterior mean, $\mu_{po}^{\nabla^2}$, and the variance, $\sigma_{po}^{\nabla^2}$, of the Laplacian, at the test point, $\mathbf{x}_i^* = [x_{i,1}^*, \dots, x_{i,M}^*]^T$, is given by (19) and (20), respectively.

$$\mu_{i,po}^{\nabla^2} = \mathbb{E}\left[\sum_{j=1}^M \frac{\partial^2 \phi(x_{i,j}^*)}{\partial x_j^2}\right]. \quad (19)$$

$$\sigma_{i,po}^{\nabla^2} = \text{Var}\left[\sum_{j=1}^M \frac{\partial^2 \phi(x_{i,j}^*)}{\partial x_j^2}\right]. \quad (20)$$

In the next section, we deal with the problem of identifying attractors and repellers of the inferred potential function.

3.4. Identifying mean attractors and repellers of the potential function

Even though it is possible to infer the potential field distribution in the entire continuous state space, it is not feasible to utilize the

inferred potential field distribution directly as an input feature for standard machine learning models, which typically operate on finite-dimensional features. Hence, we propose using mean attractor, which can be inferred from potential field distribution, as a reliable feature capable of capturing the cryptocurrency market dynamics. This section will delve into the methodology for inferring the mean attractors and repellers of the potential field.

The prior distribution over the Laplacian of the potential field (before observing the data) at any $\mathbf{x}^* \in \mathbf{X}^*$ is a univariate normal distribution, with mean, $\mu_{pr}^{\nabla^2} = 0$ and variance $\sigma_{pr}^2 \nabla^2 = \sigma^2$. Given a set of observations $\{\mathbf{x}_i\}_{i=1}^N$, the GP model in (8) can infer the posterior distributions of $\nabla^2 \phi(t, \mathbf{x}^*)$, $\forall \mathbf{x}^* \in \mathbf{X}^*$, using (19) and (20). The posterior distribution, at any $\mathbf{x}^* \in \mathbf{X}^*$, is also a univariate normal distribution with a mean, $\mu_{po}^{\nabla^2}$, and variance, $\sigma_{po}^2 \nabla^2$ computed at \mathbf{x}^* . In this paper, we use Kullback-Leibler (KL) divergence to identify significant attractors, as in Cobb, Everett, Markham, and Roberts (2018). KL divergence quantifies the degree of dissimilarity between two distributions and the KL divergence between prior and posterior distributions of the Laplacian at any location can be computed as

$$D_{KL}(p_{prior} \parallel p_{posterior}) = \frac{1}{2} \left(\frac{\sigma_{po}^2 \nabla^2 + (\mu_{po}^{\nabla^2} - \mu_{pr}^{\nabla^2})^2}{\sigma_{po}^2 \nabla^2} - 1 + \log \left(\frac{\sigma_{po}^2 \nabla^2}{\sigma_{pr}^2 \nabla^2} \right) \right). \quad (21)$$

The rationale for using KL divergence as a measure of significance for identifying attractors is the following. $\mu_{pr}^{\nabla^2} = 0$, $\forall \mathbf{x}^* \in \mathbf{X}^*$ and the value of σ_{pr} is a constant for all test points. If the prior and posterior distributions are the same, according to (21), the KL divergence value will be zero, and the new observation does not give any additional information about the trajectory, compared to the prior assumption. However, a very small value of $\sigma_{po}^2 \nabla^2$ compared $\mu_{po}^{\nabla^2}$ implies a high confidence of the model that the value of the Laplacian at the corresponding state is close to $\mu_{po}^{\nabla^2}$, resulting in a large KL divergence, according to (21). Hence, KL divergence evaluated at a state, at any given time, is proportional to its informativeness, and in our context, can be considered as a measure of the influence of a state on the trajectory.

Let $L = \{l_1, l_2, \dots, l_Q\}$, where $l_i = \mathbb{E}[\nabla^2 \phi(\mathbf{x}_i^*)] = \mu_{i,po}^{\nabla^2}$, be the set of inferred mean of Laplacian (6), at test points \mathbf{X}^* , and, $S_L = \{s_1, s_2, \dots, s_Q\}$ represent the corresponding sign of Laplacian, i.e., $s_i = \frac{l_i}{|l_i|} \in \{-1, +1\}$. Let $K = \{k_1, k_2, \dots, k_Q\}$, $k_i \in \mathbb{R}_+$ be the KL divergences of test points computed using (21). Further, we define $K^a = \{k_1^a, k_2^a, \dots, k_Q^a\} \in \mathbb{R}_+^Q$ and $K^r = \{k_1^r, k_2^r, \dots, k_Q^r\} \in \mathbb{R}_+^Q$ as (22)

$$k_i^a = \begin{cases} k_i & \text{if } s_i = +1 \\ 0 & \text{if } s_i = -1, \end{cases} \quad \text{and} \quad k_i^r = \begin{cases} 0 & \text{if } s_i = +1 \\ k_i & \text{if } s_i = -1. \end{cases} \quad (22)$$

In the following, we assume a single attractor and repeller for the potential field. The extension to multiple attractors and repellers is straightforward, as long as the number of attractors and repellers are known a priori. The mean vectors and covariance matrices of the attractors and repellers are computed as weighted mean and covariances, as in (23) and (24).

$$\mu_a = \frac{\sum_{i=1}^Q k_i^a \mathbf{x}_i^*}{\sum_{i=1}^Q k_i^a}, \quad \mu_r = \frac{\sum_{i=1}^Q k_i^r \mathbf{x}_i^*}{\sum_{i=1}^Q k_i^r}. \quad (23)$$

$$\Sigma_a = \frac{\sum_{i=1}^Q k_i^a (\mathbf{x}_i^* - \mu_a) (\mathbf{x}_i^* - \mu_a)^T}{\sum_{i=1}^Q k_i^a}, \quad \Sigma_r = \frac{\sum_{i=1}^Q k_i^r (\mathbf{x}_i^* - \mu_r) (\mathbf{x}_i^* - \mu_r)^T}{\sum_{i=1}^Q k_i^r}. \quad (24)$$

μ_a , in (23), is the mean attractor, which is the expected stable state towards which the price trajectory will converge, and Σ_a , in (24), is the corresponding covariance matrix that characterizes the uncertainty in the inferred stable state of the trajectory. Similarly, μ_r and Σ_r ,

represent the expected unstable point and the associated uncertainty, respectively.

The method of inferring the mean attractors and repellers from the time series of historic prices, as given by Eqs. (5) through (24), can be summarized with the help of the model framework diagram in Fig. 1.

4. Numerical result

The organization of this section is as follows: Section 4.1 presents a comprehensive overview of the employed dataset. Further, in Section 4.2, we validate the applicability of potential field approach for cryptocurrency market analysis using Lyapunov Stability analysis. In Sections 4.3 and 4.4, we conduct a structural analysis of the cryptocurrency market using the potential field approach in Section 3. We show that the structural analysis of the cryptocurrency market is particularly useful during cryptocurrency crash periods. Section 4.5 presents a comparison of the potential field approach with the popular wavelet coherence technique. Further, in Section 4.6, we illustrate how the inferred mean attractor can be used to improve the prediction performance of deep learning models.

4.1. Dataset description

The historical data of top ten cryptocurrencies in terms of market shares, namely, Bitcoin (BTC), Ethereum (ETH), XRP, Cardano (ADA), Algorand (ALGO), Binance coin (BNB), Polkadot (DOT), Litecoin (LTC), Polygon (MATIC) and Solana (SOL), has been obtained from coinmarketcap.com, an open-source website that provides six different features of each cryptocurrency, sampled every 5 min. The features include opening time, opening price, highest price, lowest price, closing price, and volume of transactions within a time frame of 5 min, with all prices denominated in USD.

In the subsequent sections, we illustrate how the potential field approach is beneficial for analysis of cryptocurrency market during “crash periods”. In this paper, we define a crash of a cryptocurrency as a rapid and significant drop in its market value, typically measured in terms of percentage change in price. A 15% or more decline within a period of 24 h or a few days is commonly defined as a crash (Fruehwirt et al., 2021). For example, the cryptocurrency market crash in late 2017, which affected Bitcoin, was a consequence of major hacks in Korea and Japan and the news, regarding Bitcoin bans by certain countries, appeared in social media. The 2021 crash was primarily due to China’s repression on Bitcoin mining and, the decision by Tesla, of no longer accepting Bitcoin. (Source: (Lisa, 2021)) During crash periods, it is well known that the volatility of the cryptocurrency market is high (Fruehwirt et al., 2021) and investors tend to diversify their portfolio for profit maximization and long term financial stability (Jiang et al., 2023). To simplify analysis, we focus on crash periods of BTC, the cryptocurrency with the largest market cap, for the numerical results. The details of historic BTC crashes from the year 2017 to 2021 are listed in Table 1. In this paper, we have presented the results of the crash durations of 6 to 20 January 2017, 13 April to 9 May 2021, and 7 to 9 September 2021, mentioned in the Table 1.

Variation in historic prices of various cryptocurrencies around September 2021 BTC crash duration are shown in Fig. 3. The three-day crash window, from 7 to 9 September 2021 are shaded in orange in these figures. Further, Fig. 2 shows the 7-hour candlestick plot of BTC, from 12.00am to 07.00am, on 07 September 2021. The sharp drop in BTC price from 52500 USD to 50500 USD between 4.30 am and 5.40 am is a typical instance of extreme price fluctuations of cryptocurrency.

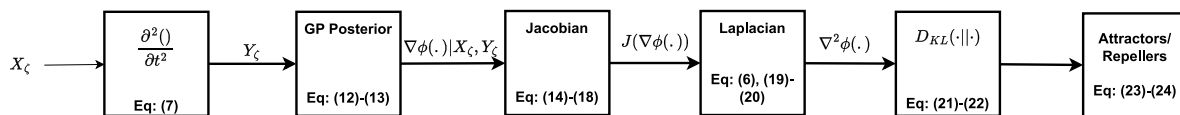


Fig. 1. Model framework diagram: A summary of the process of inferring mean attractors and repellers from the time series of cryptocurrency prices.

Table 1
Historic BTC crashes between 2017 and 2021.

S No.	Date range of crash	Duration - Days	Max value of Bitcoin (USD)	Min value of Bitcoin (USD)	% decline in price
1	2 to 15 Sep 2017	13	4939.02	3187.11	35.47
2	8 to 12 Nov 2017	4	7690	6100.03	20.67
3	6 to 20 Jan 2018	19	17173.97	9055.03	47.27
4	26 Jun to 12 Jul 2019	16	13964.64	9754.25	30.15
5	13 Apr to 9 May 2021	26	64702.02	47135.68	27.15
6	7 to 9 Sep 2021	2	52866.65	43088.74	18.5

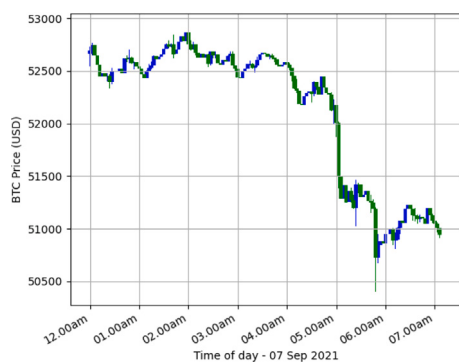


Fig. 2. Candle Stick diagram of Bitcoin from 12:00 am to 7:00 am on 7 Sep 2021. The sharp drop in BTC price from 52500 USD to 50500 USD between 4.30 am and 5.40 am is a typical instance of extreme price fluctuations of cryptocurrency.

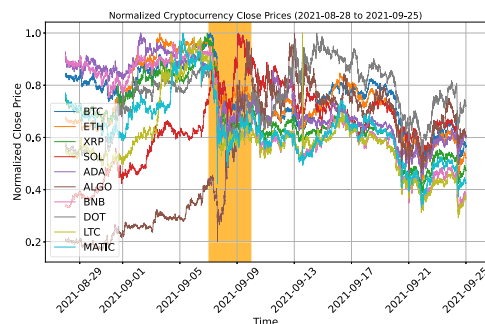


Fig. 3. Historic prices of 10 different cryptocurrencies from 21 Aug to 25 Sep 2021. The BTC crash duration is marked in orange. Prices of cryptocurrencies are individually normalized between 0 and 1 during the observation window.

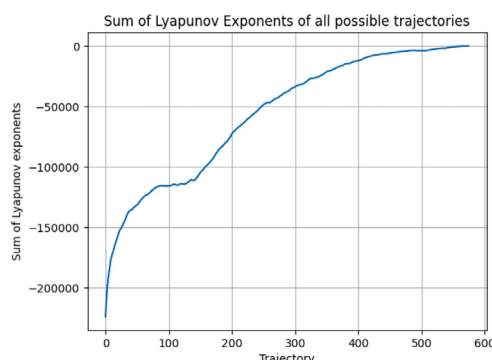


Fig. 4. Lyapunov exponents of trajectories during 72-hour Bitcoin Crash window — April 2021.

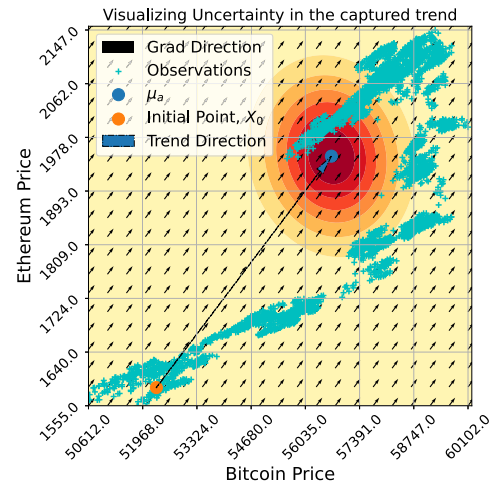


Fig. 5. Market trend captured using the proposed approach before crash period (25 March to 9 April 2021).

4.2. Existence of a valid potential field for the cryptocurrency market

In this section, we investigate the validity of the potential field model in (2), using Lyapunov stability analysis (Algorithm 1) and Recurrence Quantification Analysis (RQA)⁴ (Webber, Jr. & Zbilut, 2005). As the inferences regarding Lyapunov stability are identical in all cases, we present only the results for the 72-hour observation period during the Bitcoin Crash, from 8 to 10 September 2021. Fig. 4 displays the Lyapunov exponents (L , the output of Algorithm 1), of the trajectory, arranged in ascending order. The maximum Lyapunov exponent, λ_1 , is less than zero, indicating the presence of a time-varying, nonlinear potential function with an attractor (Biswal & Dasgupta, 2002; Yuan et al., 2013). In the subsequent sections, we use the inferred mean attractor and the associated uncertainty measure to analyse the market trends and structural dependencies during various BTC crash durations.

4.3. Cryptocurrency market analysis — Bitcoin and Ethereum

For the convenience of visualization, we start with BTC and ETH, the two major cryptocurrencies in terms of market cap.

Figs. 5, 6, and 7, where the horizontal axes represent the USD prices of Bitcoin, while the vertical axes represent the USD prices of Ethereum, shows the structural dependencies, obtained through the potential field approach in Section 3, of BTC and ETH before (25 March 2021 to

⁴ The details of the RQA analysis are provided in Appendix A.

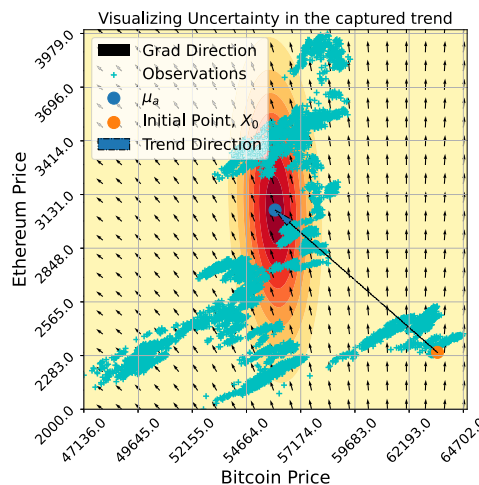


Fig. 6. Market trend captured using the proposed approach during crash period (13 April to 19 May 2021).

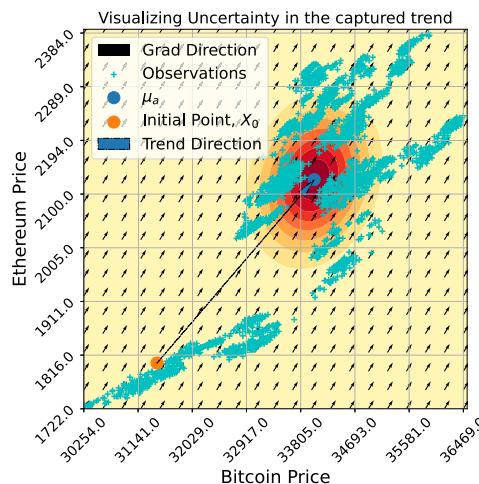


Fig. 7. Market trend captured using the proposed approach after crash period (26 June to 14 July 2021).

09 April 2021), during (13 April 2021 to 09 May 2021), and after (21 June 2021 to 07 July 2021) the April 2021 Bitcoin crash. The GP in (8) was trained⁵ using the price trajectories of the respective windows, and the potential gradient and its Jacobian were inferred in a finite mesh grid of test points in the state space using (12) and (17), respectively, for all windows. The vector lines corresponding to the inferred posterior mean of potential gradient, as in (12), in the mesh grid, are shown as arrows in the state space in Figs. 5, 6, and 7. Further, (6) was used to compute the Laplacian at the test points. Subsequently, the KL divergence between the prior and posterior distributions of the Laplacian at all test points are evaluated using (21). Finally, the mean of the mean attractor ($\mu_a = [\mu_{BTC}, \mu_{ETH}]^T$) and covariance matrix (Σ_a) in the respective windows, were obtained using (23) and (24). Cyan markers on the state space indicate the states of the observed price trajectory, during the respective observation windows. The initial state of an observation window will be denoted as $x_0 = [x_{BTC,0}, x_{ETH,0}]^T$, and is marked in orange. The blue markers represent the posterior mean of the inferred mean attractors of each window. The concentric

⁵ The training process of GP involves finding the values of the hyperparameters and the noise variance that best fit the training data. This is done by maximizing the log marginal likelihood of the data given the hyperparameters.

ellipses, the contours⁶ of the Gaussian cloud $\mathcal{N}(\mu_a, \Sigma_a)$, represent the uncertainty in the inference of mean attractor.

The structural dependency inferences related to cryptocurrency market such as market trend, volatility and its associated uncertainty, convergence and market stabilization, and visualizing shift in market trends are discussed in Section 4.3.1 to Section 4.3.5.

4.3.1. The trend lines

Trend Line, a directed line segment from the initial state to the mean attractor, in Figs. 5, 6, and 7, provides insights into the trends in price corrections, the overall correlation during the observation window and the possible direction of asset shift, between BTC and ETH. The magnitude and inclination of trend lines, in all the crash durations of interest, are quantified in Table 2.

Before the crash of April 2021, the Bitcoin price showed a rapid increase, which resulted in a bubble⁷ formation, as characterized by a trend line inclination of ~ 60 degrees⁸, in Fig. 5. During the crash, the bubble burst, leading to a substantial negative correction in the Bitcoin price, which fell on an average by $-10000USD$, characterized by ~ 135 degrees inclination of trend line in Fig. 6. The Bitcoin price started showing positive corrections during the recovery period after the crash, as depicted in Fig. 7.

In addition, it can be observed from Table 2 that the price of Ethereum (ETH) has undergone positive price corrections of approximately $+350USD$, $+650USD$, and $+300USD$, respectively, before, during and after the BTC crash of April 2021. Notably, during the Bitcoin (BTC) market downturn, there was a substantial high positive correction observed in the price of Ethereum, as shown in Fig. 6. This trend suggests a possible asset shift from Bitcoin to Ethereum during the Bitcoin crash period, whereby individuals exchanged their BTC for ETH. This shift in asset allocation increased the demand for ETH, leading to a favourable effect on its price.

4.3.2. Uncertainty in mean attractor and confidence of price correction

The uncertainty in the inferred mean attractor is characterized by the Gaussian cloud, $\mathcal{N}(\mu_a, \Sigma_a)$, contours of which in state space are represented as concentric ellipses centred at the mean attractors, in Figs. 5, 6, and 7. Here, μ_a and Σ_a are obtained using (23) and (24), respectively. The multivariate Gaussian probability density function $\mathcal{N}(\mu_a, \Sigma_a)$ quantifies the likelihood of the inferred mean attractors being located within this Gaussian cloud.

We can infer the confidence of price correction (whether its an uptrend or downtrend of price) as the probabilities of positive and negative price corrections of the cryptocurrencies, starting from the initial state, x_0 , based on the inferred distribution $\mathcal{N}(\mu_a, \Sigma_a)$. The probability of positive price correction for BTC is computed as $P(X_{BTC} > x_{BTC,0})$, as in (25),

$$P(X_{BTC} > x_{BTC,0}) = \int_{x_{BTC,0}}^{\infty} f_{X_{BTC}}(x) dx, \quad (25)$$

where, $f_{X_{BTC}}(x)$ is the probability density function of BTC price and $X_{BTC} \sim \mathcal{N}(\mu_{BTC}, \sigma_{BTC})$. The probability of negative correction is computed as $1 - P(X_{BTC} > x_{BTC,0})$. Similarly, the probabilities pertaining to the ETH price corrections are also computed. These findings are quantified and summarized in Table 2. Throughout all crash periods,

⁶ Contours of a multivariate Gaussian probability density function, are lines or surfaces that connect the points of equal probability density. The contours of this distribution will be ellipses if the covariance matrix is positive semidefinite

⁷ When an asset is traded at a price exceeding that asset's intrinsic value, mostly due to speculations. Speculation in trading terminology refers to the investment in the market, in the hope of gain but with the risk of loss. Further, independent of its market price, the intrinsic value of a cryptocurrency is determined by its utility, scarcity and technological application (Fruehwirt et al., 2021).

⁸ Percentage positive price correction of BTC is greater than that of ETH

Table 2

Characterizing trends and uncertainties — BTC and ETH.

Crash window	Trend line magnitude (USD)		Trend line direction	Probability of negative correction		Probability of positive correction	
	BTC	ETH		BTC	ETH	BTC	ETH
Dec 2017	Before	2893.32	125.429	40°	0	0	1
	During	-3468.254	281.435	135°	1	0	0
	After	2337.132	223.258	50°	0	0	1
Apr 2021	Before	4168.778	373.964	60°	0	0	1
	During	-7359.387	542.325	135°	1	0	0
	After	2371.57	326.296	45°	0	0	1
Sep 2021	Before	293.305	21.645	45°	0	0	1
	During	-229.072	76.894	120°	1	0	0
	After	-79.729	-7.862	218°	0	0	1

the price of BTC exhibited notable positive corrections prior to the crash, which led to the formation of a speculative bubble. Subsequently, a sudden negative correction ensued during the crash itself, ultimately followed by a gradual positive correction during the recovery phase. It is evident from the results in [Table 2](#) that the inferred mean attractor correctly characterizes the price correction trends, before, during and after various crash durations, with a high degree of confidence.

4.3.3. Characterizing the volatility and correlation of cryptocurrencies

The contours of the posterior covariance of the mean attractor is a hyper-ellipsoid, the principal axes of which can give insights about the volatility of cryptocurrencies and the correlation between individual components of the price vector ([Murphy, 2012](#)). In 2-dimensional case, as in [Figs. 5 and 7](#), involving BTC and ETH, when the principal axis and the horizontal axis (BTC price) form an acute angle⁹, it indicates a positive correlation between Bitcoin (BTC) and Ethereum (ETH). Conversely, as in [Fig. 6](#), an obtuse angle suggests a negative correlation between the cryptocurrencies. Horizontally, or vertically oriented principal axis, suggest no correlation between the individual components of the price vector. This orientation can be obtained from the principal component (the eigen vector corresponding to the largest eigen value) of the covariance matrix Σ_a ([Murphy, 2012](#)). Furthermore, the length of principal axis, which is the largest eigen value of Σ_a , being proportional to the dispersion in price, can quantify the volatility of cryptocurrencies. The principal components and the corresponding eigen values for various crash durations are presented in [Table 3](#).

Several aspects related to the volatility behaviour of BTC and ETH can be inferred from [Figs. 5, 6, and 7](#), and [Table 3](#). The volatility increases during crash periods, as quantified by the eigen values corresponding to the principal component of the covariance matrix (Σ_a). From [Table 3](#), we can note that the eigenvalues exhibit a change in value, specifically 0.047 and 0.069, correspondingly, prior to (25 March to 9 April, 2021) and during (13 April to 9 May, 2021) the April 2021 BTC crash. This change indicates a significant increase in volatility during the April 2021 crash period. Further, after the April 2021 crash duration (26 June to 14 July 2021), the eigen value reduced to 0.067, indicating a reduction in volatility, during the market recovery, after the April 2021 crash. Similar results can be inferred for September 2021 BTC crash, from [Table 3](#). In contrast to the April 2021 and September 2021 BTC crashes, we observe that the eigenvalue increased from 0.051 during the crash to 0.061 after the crash of January 2018. This increase in volatility, lies in the sustained period during which the BTC price remained at the crashed value, lasting nearly one year following the January 2018 crash. Moreover, the recovery of the cryptocurrency market from this crash occurred only in early 2019.

Further, it can be observed from [Table 3](#) that, during the period of 25 March to 9 April 2021, prior to the BTC crash, the principal axis made an orientation of 17° with respect to the BTC axis. This orientation

indicates a slight positive correlation between BTC and ETH, as both prices demonstrated a positive trend. In contrast, during the crash period from 13 April to 9 May, the principal axis and BTC axis formed an angle of 95.7°, indicating a slight negative correlation between BTC and ETH. This finding aligns with the fact that while BTC experienced a significant negative correction during the crash, ETH exhibited a positive correction. Additionally, from 26 June to 14 July, after the crash, the principal axis exhibited an angle of 46° with the BTC axis, indicating a very high positive correlation between BTC and ETH. These observations suggest that the structural dependency between BTC and ETH increased considerably following the April 2021 crash. Moreover, by combining the insights regarding price correction trends ([Table 2](#)), direction of inferred potential gradient ([Figs. 5 through 7](#)) and the information on structural dependence ([Table 3](#)), it is possible to infer a potential shift of assets from BTC to ETH during the crash period of April 2021.

4.3.4. Convergence characteristics and market stabilization

In this section, we empirically analyse the convergence property of the cryptocurrency price trajectory towards the inferred mean attractor, and the temporal evolution of the mean attractor. The cryptocurrency market is deemed to be stabilized when the price trajectory falls within a distance of σ_a from the mean attractor, as implied by [\(26\)](#).

$$\|\mathbf{x}_n - \mu_a\| \leq \sigma_a, \text{ where } n = 1, \dots, N, \quad (26)$$

where, \mathbf{x}_n is the state of the trajectory at time t_n . The quantity, $\sigma_a = |\Sigma_a|^{\frac{1}{2}}$ (Σ_a is inferred from [\(24\)](#)), represents the area of the Gaussian cloud, centred at the mean attractor, that encloses 68.27% of the total probability mass of the multivariate Gaussian distribution, $\mathcal{N}(\mu, \Sigma_a)$. [Figs. 8 to 10](#), depict the convergence behaviour of cryptocurrency market dynamics over time, indicating the timeline of market stabilization. The horizontal axis represents time, and the vertical axis represents the normalized Euclidean distance from the attractor. The horizontal lines coloured in red, in [Figs. 8 to 10](#), depict the inferred uncertainty, which is the normalized standard deviation, σ_a , of the location of the mean attractor. The blue graph represents the distance between the states of trajectory from mean attractor as a function of time. The orange and green graphs represent the absolute distances of BTC price and ETH price respectively from the corresponding components of mean attractor. As a result of the market's intrinsic volatility, the price may display temporary divergences from the attractor. However, on average, during the convergence period, the region which is highlighted in orange, in [Figs. 8 through 10](#), the price is observed to return and remain within a distance of σ_a from the mean attractor. If the Euclidean distance between the trajectory's states and the inferred mean attractor consistently exceeds σ_a , it indicates a displacement of the attractor's position caused by a shift in market trend.

[Table 4](#) presents the BTC and ETH components of the inferred mean attractor, the onset and ending time of convergence and duration of convergence for different observation windows. For instance, it can be observed that during the BTC market downturn in April 2021, the price trajectory approached the mean attractor within a distance of σ_a on

⁹ In [Figs. 5, 6, and 7](#), different scales are used for horizontal and vertical axes. Refer [Table 3](#), for exact inclination of principal axis.

Table 3
Structural dependence during convergence — BTC and ETH.

Observation window	Eigen Value	Eigen Vector	Phase (BTC (x) and ETH (y))
7 to 18 Dec 2017	0.025	[0.605, -0.796]	128°
6 to 20 Jan 2018	0.051	[-0.553, -0.833]	56.42°
6 to 20 Feb 2018	0.066	[0.720, 0.693]	43.88°
25 Mar to 9 Apr 2021	0.047	[0.956, 0.293]	17.01°
13 Apr to 9 May 2021	0.069	[0.099, -0.995]	95.7°
26 Jun to 14 Jul 2021	0.067	[-0.691, -0.723]	46.33°
29 to 30 Aug 2021	0.025	[-0.645, -0.764]	49.8°
7 to 9 Sept 2021	0.031	[0.715, 0.698]	44.3°
25 to 26 Sept 2021	0.003	[-0.660, -0.751]	48.74°

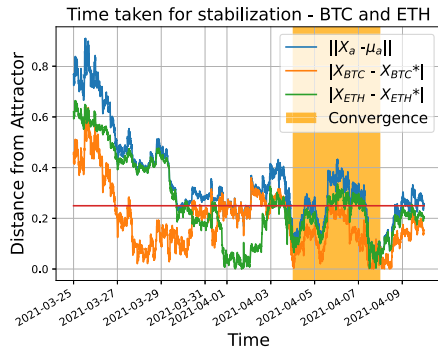


Fig. 8. Convergence to attractor — Before crash (25 March to 9 April 2021).

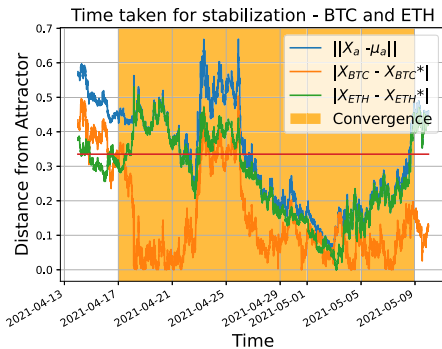


Fig. 9. Convergence to attractor — During crash (13 April to 19 May 2021).

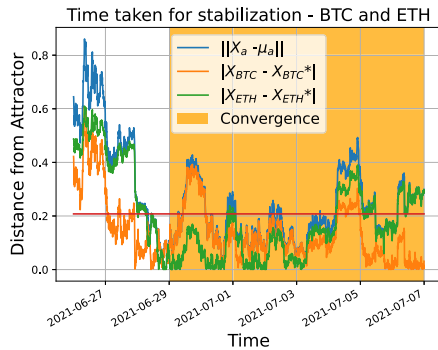


Fig. 10. Convergence to attractor — After crash (26 June to 14 July 2021).

April 16, 2021. The trajectory remained in this vicinity until May 5, 2021, indicating convergence towards the mean attractor. However, the trajectory deviated away from the mean attractor (inferred during the crash window), which can be attributed to the rebound in the BTC price during the first week of May 2021.

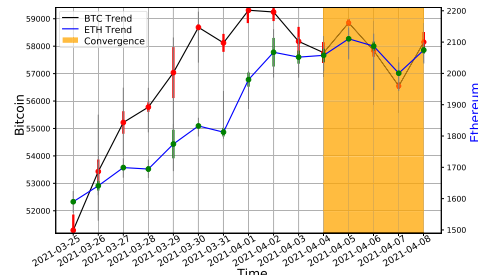


Fig. 11. Temporal evolution of attractor — Before crash (25 March to 9 April 2021).

4.3.5. Temporal advancement of attractors — visualizing the shift in market trend

Figs. 11 through 13 depict the temporal evolution of attractors across distinct 1-day sub-windows within the observation windows presented in Figs. 5 through 7, respectively. The BTC and ETH components of the mean attractor, as defined by Eq. (23), are displayed separately with accompanying error plots, representing the associated uncertainties. The uncertainty, $\sigma_a = |\Sigma_a|^{\frac{1}{2}}$, obtained using Eq. (24), over the respective 1 day subwindows. The shaded areas correspond to the region of convergence, similar to Figs. 8 through 10. The movement of attractors effectively captures the BTC price bubble formation prior to the crash in Fig. 11, the severe negative correction of BTC price during the crash in Fig. 12, and the recovery of BTC price after the crash in Fig. 13. Additionally, the positive price correction of ETH price during all three windows is evident from Figs. 11 through 13.

Each time interval in the cryptocurrency's observation sub-windows is represented by an error bar, which provides useful information on the corresponding volatility. The error bar captures the regions around μ_{BTC} and μ_{ETH} bounded by $\pm\sigma_{BTC}$ and $\pm\sigma_{ETH}$, respectively. An increase in the size of the error bar indicates higher uncertainty and, hence, higher volatility, while a decrease in the size of the error bar indicates lower volatility. For instance, the error bars at the mean attractor points in Figs. 11 and 13 are relatively small compared to the mean value across the subwindows. However, during the window spanning from April 16 to 17, 2021, as shown in Fig. 12, a significantly wide error bar can be observed for BTC, indicating a drastic negative correction of BTC price by 16% in just two days, at the onset of the BTC market downturn.

4.4. Cryptocurrency market analysis — more than 2 cryptocurrencies

It is relatively easy to extend the analysis to include more than two cryptocurrencies simultaneously. However, representing scenarios with dimensions greater than two using a 2D plot, as done in Figs. 5 through 7, is impractical. A more practical approach is to use a facet of figures that illustrate pairwise interactions. Specifically, we have considered BTC, ETH, and XRP for the 3 cryptocurrency case, while all 10 cryptocurrencies mentioned in Section 4.1 are included in the 10-dimensional case. The Figs. 14 through 25 depict the

Table 4

Convergence characteristics — BTC and ETH.

Observation window	BTC component of mean attractor	ETH component of mean attractor	Onset of convergence	End of convergence	Convergence duration
7 to 18 Dec 2017	16 663.32	534.42	Dec 11 2017	Dec 12 2017	1 day
6 to 20 Jan 2018	13 450.745	1236.215	Jan 08 2018	Jan 16 2018	8 days
6 to 20 Feb 2018	8898.132	877.248	Feb 08 2018	Feb 14 2018	6 days
25 Mar to 9 April 2021	58 138.71	1925.75	Apr 04 2021	Apr 08 2021	4 days
13 April to 9 May 2021	56 142	2841	Apr 16 2021	May 08 2021	22 days
26 June to 14 July 2021	33 823	2128	Jun 28 2021	Jul 12 2021	14 days
29 to 30 Aug 2021	48 554.235	3205.435	Aug 28 2021	Aug 29 2021	1 day
7 to 9 Sept 2021	46 434	3476	Sep 07 2021	Sep 09 2021	2 days
25 to 26 Sept 2021	42 589.74	2913.388	Sep 25 2021	Sep 26 2021	1 day

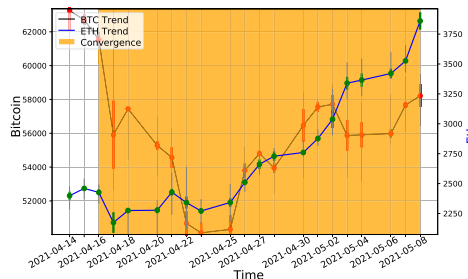


Fig. 12. Temporal evolution of attractor — During crash (13 April to 19 May 2021).

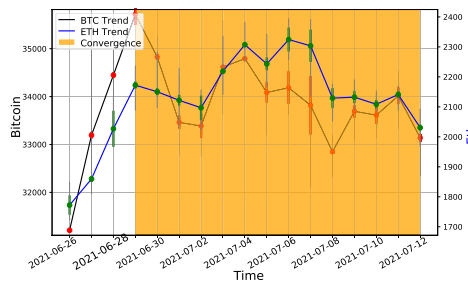


Fig. 13. Temporal evolution of attractor — After crash (26 June to 14 July 2021).

convergence characteristics and temporal evolution of attractors for 3 cryptocurrencies and 10 cryptocurrencies. Specifically, BTC, ETH, and XRP are considered for the 3 cryptocurrency case, while all 10 cryptocurrencies mentioned in Section 4.1, are included in the 10-dimensional case. To aid visualization, the prices of cryptocurrencies in Figs. 14 to 25 are normalized using max-min normalization. Whenever distance measures are mentioned, they refer to the distance between the normalized prices.

The results obtained for the 3D and 10D analyses are consistent with our 2D analysis inference, as far as BTC and ETH are concerned. The 3D and 10D results notably capture the consistent positive corrections in ETH price across all three windows, namely, before, during and after April 2021 BTC crash duration. Furthermore, they correctly represent the formation of the BTC bubble before the crash, the substantial negative correction of BTC price during the crash, and the recovery of BTC price following the crash.

The convergence characteristics, trend characterization and structural dependence of BTC-ETH-XRP case (for BTC crash durations, namely, April 2021 and September 2021) are summarized in Tables 5–7, respectively. It can be observed in comparison with 2-dimensional case (BTC-ETH) that the duration of convergence has substantially reduced in the three-dimensional case. For example, during April 2021 crash window, a crash that has sustained for a long period, the duration of convergence were 20 and 8 for 2-dimensional and 3-dimensional cases respectively. This is a consequence of very high volatility of XRP.

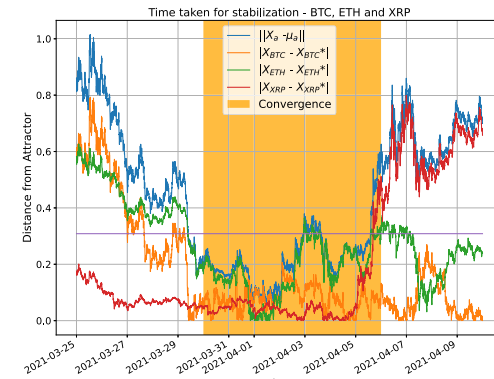


Fig. 14. Convergence to attractor — Before crash – 3D case (25 March to 9 April 2021).

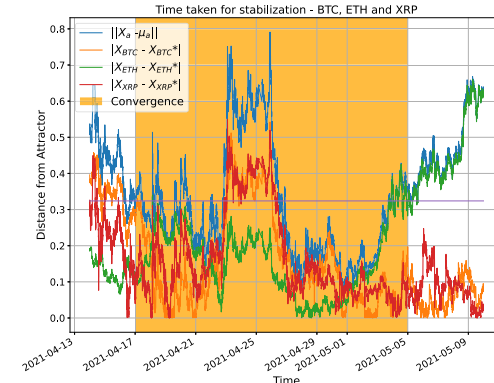


Fig. 15. Convergence to attractor — During crash – 3D case (13 April to 19 May 2021).

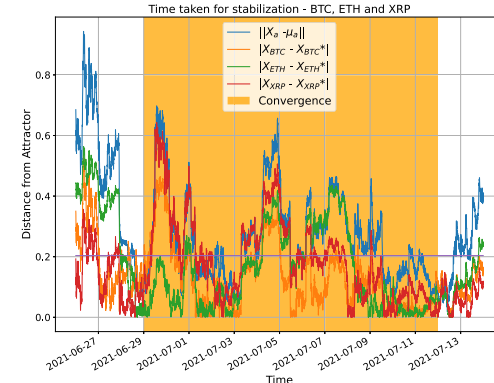


Fig. 16. Convergence to attractor — After crash – 3D case (26 June to 14 July 2021).

Table 5

Convergence properties during various observation windows.

Observation window	BTC component of mean attractor	ETH component of mean attractor	XRP component of mean attractor	Onset of convergence	End of convergence	Convergence duration
25 Mar to 9 April 2021	58 138.71	1925.75	0.59	Mar 29 2021	Apr 05 2021	7 days
13 April to 9 May 2021	56 642.38	2675.17	1.497	Apr 16 2021	May 03 2021	17 days
26 June to 14 July 2021	33 989.65	2146.28	0.65	Jun 28 2021	Jul 12 2021	14 days
29 to 30 Aug 2021	48 888.295	3238.814	1.1533	Aug 29 2021	Aug 30 2021	1 day
7 to 9 Sept 2021	46 400.85	3467.33	1.101	Sep 07 2021	Sep 09 2021	2 days
25 to 26 Sept 2021	42 583.55	2915.80	0.941	Sep 25 2021	Sep 26 2021	1 day

Table 6

Characterizing trends and uncertainties — BTC, ETH and XRP.

Crash window	Trend Line magnitude (USD)			Probability of negative correction			Probability of positive correction			
	BTC	ETH	XRP	BTC	ETH	XRP	BTC	ETH	XRP	
Apr 2021	Before	5750.54	344.61	0.11	0	0	0.01	1	1	0.99
	During	-6977.6	368.76	-0.31	1	0	1	0	1	0
	After	2586.03	343.65	0.04	0	0	0.01	1	1	0.99
Sep 2021	Before	627.364	55.024	0.0249	0	0	0	1	1	1
	During	-279.2	56.94	-0.01	1	0	0.9997	0	1	0.0003
	After	-85.92	-5.45	0.0004	1	1	0.489	0	0	0.511

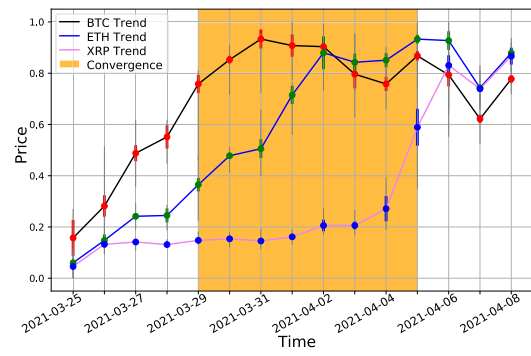


Fig. 17. Temporal evolution of attractor – Before crash – 3D case (25 March to 9 April 2021).

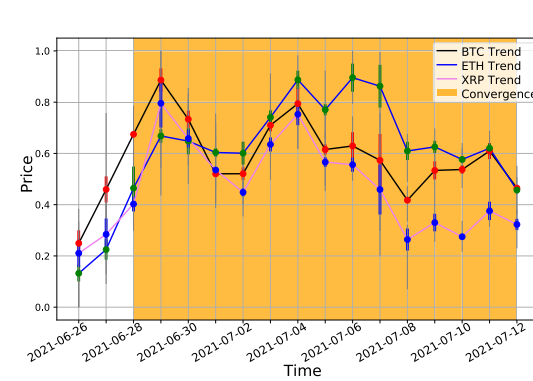


Fig. 19. Temporal evolution of attractor – After crash – 3D case (26 June to 14 July 2021).

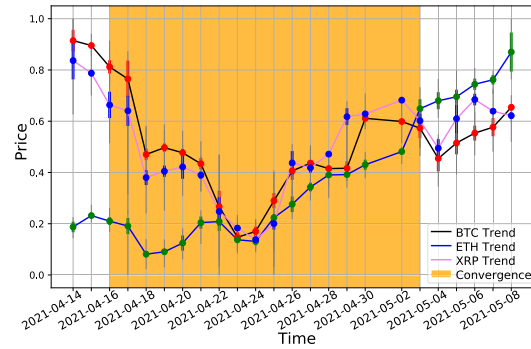


Fig. 18. Temporal evolution of attractor - During crash – 3D case (13 April to 19 May 2021).

Similarly, the probability of positive or negative corrections are almost certain for BTC and ETH, while there is a significant uncertainty in the case of XRP ([Table 6](#)). Further, [Table 7](#) quantifies the structural dependence between BTC, ETH and XRP and the volatility. Parameters, namely, market trend, uncertainty, pairwise correlation, and volatility can be effortlessly quantified for any number of dimensions, and the summary of 3D cases, for all crash durations, other than April 2021 and September 2021, are included as tables in online appendix (supplementary material).

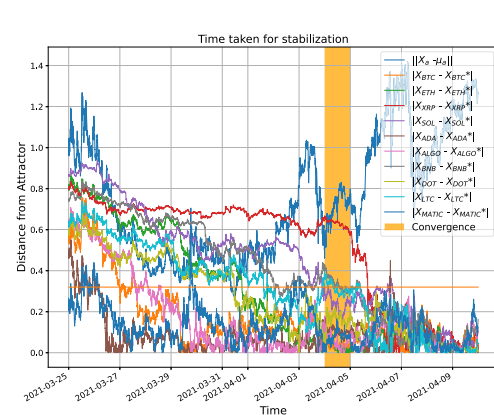


Fig. 20. Convergence to attractor – Before crash – 10D case (25 March to 9 April 2021).

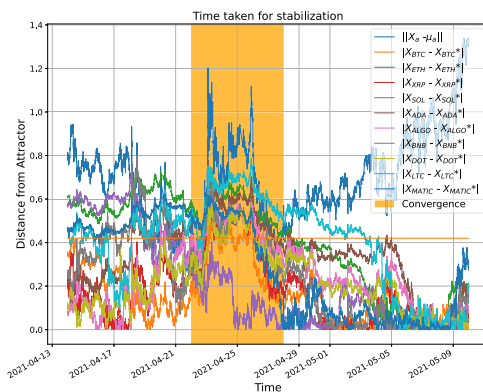
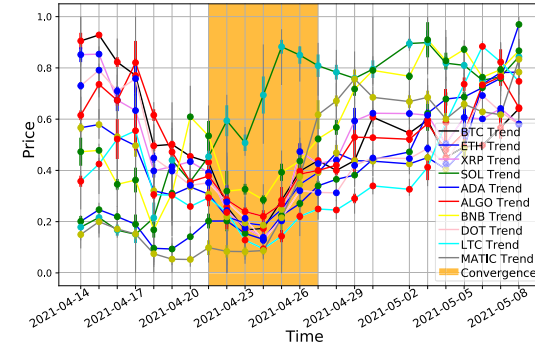
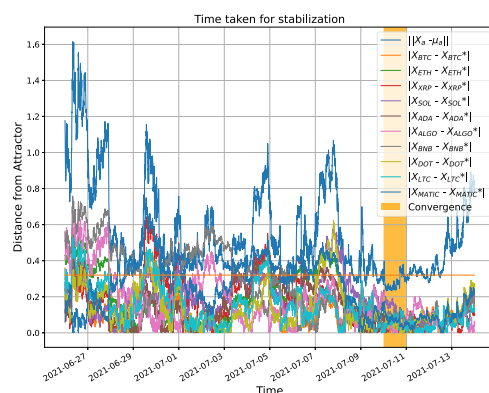
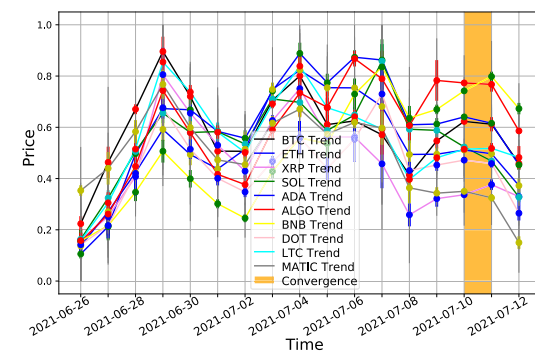
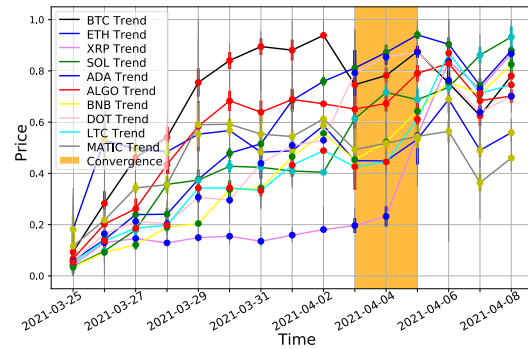
4.5. Comparison with wavelet coherence technique

In this section, we analyse the consistency of the structural dependence information inferred using the potential field approach, with the results obtained using the popular wavelet coherence based technique for analysing structural dependence between any given pairs of cryptocurrencies (Qiao et al., 2020). Wavelet coherence technique analyse the dependency between two time series, in the time-frequency

Table 7

Structural dependence during convergence — BTC, ETH and XRP.

Observation window	Eigen value	Eigen vector	Phase (BTC - ETH)	Phase (ETH - XRP)	Phase (BTC - XRP)
25 Mar to 9 April 2021	0.036	[0.080, 0.758, 0.646]	83.93°	40.45°	7.04°
13 April to 9 May 2021	0.044	[-0.814, 0.362, -0.453]	156.01°	129°	27.5°
26 June to 14 July 2021	0.012	[-0.299, 0.947, 0.109]	107.5°	11.51°	24°
29 to 30 Aug 2021	0.001	[0.088, 0.996, 0.00]	84.9°	0.00°	0.00°
7 to 9 Sept 2021	0.008	[-0.466, 0.727, 0.503]	122.67°	34.66°	132.8°
25 to 26 Sept 2021	0.015	[-0.176, 0.0006, 0.984]	0.00°	90°	45.6°

**Fig. 21.** Convergence to attractor – During crash – 10D case (13 April to 19 May 2021).**Fig. 24.** Temporal evolution of attractor - During crash – 10D case (13 April to 19 May 2021).**Fig. 22.** Convergence to attractor – After crash – 10D case (26 June to 14 July 2021).**Fig. 25.** Temporal evolution of attractor – After crash – 10D case (26 June to 14 July 2021).**Fig. 23.** Temporal evolution of attractor – Before crash – 10D case (25 March to 9 April 2021).

domain, by extending the concept of cross-correlation to the wavelet transform framework.

The cross wavelet transform of two time series $x(t)$ and $y(t)$ is given by

$$W_{xy}(a, b) = \frac{1}{a} \int_{-\infty}^{\infty} x(t) \cdot y^*(\frac{t-b}{a}) \cdot \psi^*(\frac{t-b}{a}) dt, \quad (27)$$

where, $W_{xy}(a, b)$ represents the cross wavelet coefficients as a function of scale (frequency) a and translation (time) b . As in Qiao et al. (2020), we use a Morlet wavelet, given by (28),

$$\psi(t) = \pi^{-1/4} e^{i\omega_0 t} e^{-t^2/2}, \quad (28)$$

where, ω_0 is the central frequency of the wavelet. Further, wavelet coherence R_{xy} between the two time series $x(t)$ and $y(t)$ can be computed as,

$$R_{xy}^2 = \frac{|S(a^{-1} W_{xy}(a, b))|^2}{S(a^{-1} |W_x(a, b)|^2) S(a^{-1} |W_y(a, b)|^2)}. \quad (29)$$

In (29), $S(\cdot)$ is the smoothing function, for example, weighted running average in both time and frequency directions. Further, $W_x(a, b)$ and $W_y(a, b)$ are continuous wavelet transforms of $x(t)$ and $y(t)$, respectively. It is easy to see that $0 \leq R_{xy}^2 \leq 1$. When the value of R_{xy}^2 is close to zero, it indicates that the correlation between the time series is weak, whereas, a value of R_{xy}^2 close to 1 signifies a strong correlation. The coherence phase, $\tan^{-1} (\text{Re}(W_{xy}(a, b)) / \text{Im}(W_{xy}(a, b)))$, represents the

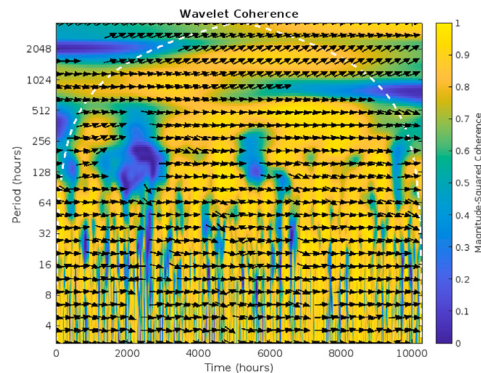


Fig. 26. Wavelet coherence between BTC and ETH prices before crash period (25 March to 9 April 2021).

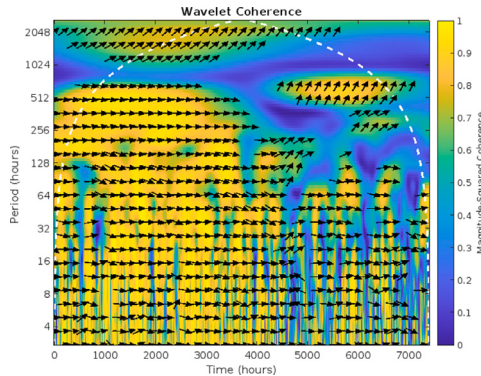


Fig. 27. Wavelet coherence between BTC and ETH prices during crash period (13 April to 19 May 2021).

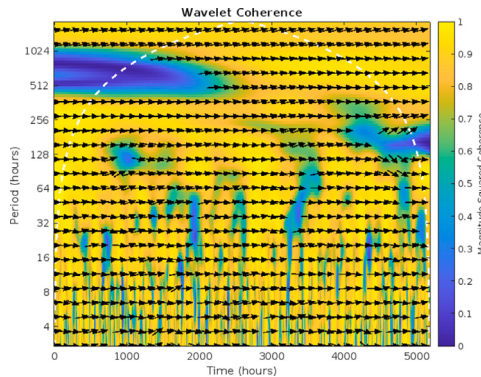


Fig. 28. Wavelet coherence between BTC and ETH prices after crash period (26 June to 14 July 2021).

phase angle associated with the coherence between the two time series at different time-frequency points. It gives information about the time lag or phase relationship between the two time series.

The wavelet coherence plots, Figs. 26 through 28, show the coherence, R_{xy}^2 (computed using (29)), between the time series of BTC and ETH prices, as a function of frequency and time, along with the coherence phase. The horizontal axis of the wavelet coherence plots represent the timescale, and the vertical axis represent the time period (inverse of frequency) scale of coherence. The strength of correlation is indicated by the colour map, with yellow indicating, $R_{xy}^2 = 1$, and blue indicating, $R_{xy}^2 = 0$. For each frequency and time combination, the coherence phase determines the direction of arrows in the wavelet coherence plots. A positive correlation between the two time series is

represented by an arrow directed towards the right, while a negative correlation is denoted by an arrow pointing towards the left. Additionally, the orientation of the arrow (upward or downward) provides information about the temporal relationship between the two signals. Specifically, if the arrow points upwards, it indicates that the first time series, BTC price, leads the second time series, ETH price, at that particular time-frequency point. Conversely, if the arrow points downwards, it signifies that the ETH price leads the BTC price at that specific time and frequency. Arrows present in the lower time period horizon indicate short term dependency, whereas arrows in the upper time period horizon shows long term dependency, between BTC and ETH price variations.

The inferences regarding structural dependence, between BTC and ETH, drawn from Figs. 26 through 28 can be summarized as follows: (i) Before the crash, from 25 March to 9 April 2021, the wavelet coherence analysis (Fig. 26) reveals predominant yellow regions and right-directed arrows, indicating a positive correlation between BTC and ETH prices. (ii) During the crash period, from 13 April to 19 May 2021, significant blue regions appear (Fig. 27), suggesting a very low correlation between BTC and ETH prices. Moreover, the presence of left-up arrows during the crash period indicates a negative correlation. This negative correlation pattern signifies that when BTC prices dropped, there was a subsequent gain in ETH prices, suggesting a shift of assets from BTC to ETH. (iii) After the crash (Fig. 28), from 26 June to 14 July 2021, the wavelet coherence analysis shows an increased yellow area compared to the other two cases, along with a rightward arrow. This indicates a strengthened correlation between BTC and ETH prices during the post-crash duration. In summary, the structural dependence between BTC and ETH has heightened after the crash event.

The aforementioned inferences obtained from the popular wavelet coherence approach are consistent with the inferences on structural dependence, as in Table 3, made using the proposed potential field approach (Section 4.3.3).

4.6. Improvement in error performance of LSTM based prediction techniques when mean attractor is used as an input feature

Many deep learning models are available in literature that predict cryptocurrency price based on historic price information. Tanwar et al. (2021) presented an LSTM based model which exploits the interdependence between LTC and BTC to improve the performance, in terms of MSE and MAE of LTC price prediction, compared to the LSTM models that considers historic LTC prices alone as input features. The architecture used in Tanwar et al. (2021) is shown in Fig. 29. This LSTM model takes in two inputs and generates the LTC price as output. The first input is a historical record of LTC's daily closing prices, $\zeta_{1:N} = \{p_1, p_2, \dots, p_N\}$, while the second input is a historical record of some attribute, $\theta_{1:N} = \{\tau_1, \tau_2, \dots, \tau_N\}$, that can capture the daily market trend of BTC, the parent coin. In Tanwar et al. (2021), the attribute used for the second input is the BTC price direction, $\theta_{1:N}^{dir} = \{\tau_1^{dir}, \tau_2^{dir}, \dots, \tau_N^{dir}\}$, which is determined by comparing the daily mean price of BTC to its open price. If the mean price is greater than the open price, the corresponding BTC price direction attribute, τ_i^{dir} , is set to 1; otherwise, it is set to -1.

However, the BTC price direction attribute used in Tanwar et al. (2021), depends on the mean price, of a time series, that exhibits fluctuations, due to significant volatility in the market, and hence, in this paper we argue that the mean attractor inferred from the time series is a more reliable indicator of the market trend and structural dependence than the BTC price direction attribute. We propose, using the mean attractor of the daily price window (computed as in (23)), $\theta_{1:N}^{att} = \{\tau_1^{att}, \tau_2^{att}, \dots, \tau_N^{att}\}$, instead the BTC price direction attribute, $\theta_{1:N}^{dir}$, as the second input to the model in Tanwar et al. (2021).

To compare the error performance of the existing and proposed approaches, we used historical data of BTC and LTC closing prices

Table 8

LSTM based price prediction — MSE performance comparison.

	1 Day	2 Day	3 Day	5 Day	7 Day	10 Day	12 Day	13 Day	14 Day
Mean Existing	0.073	0.081	0.089	0.106	0.139	0.173	0.201	0.213	0.225
STD Existing	0.147	0.179	0.207	0.27	0.355	0.435	0.471	0.487	0.499
Mean Proposed	0.059	0.067	0.074	0.090	0.107	0.143	0.159	0.224	0.266
STD Proposed	0.139	0.17	0.202	0.266	0.347	0.486	0.53	1.259	1.791

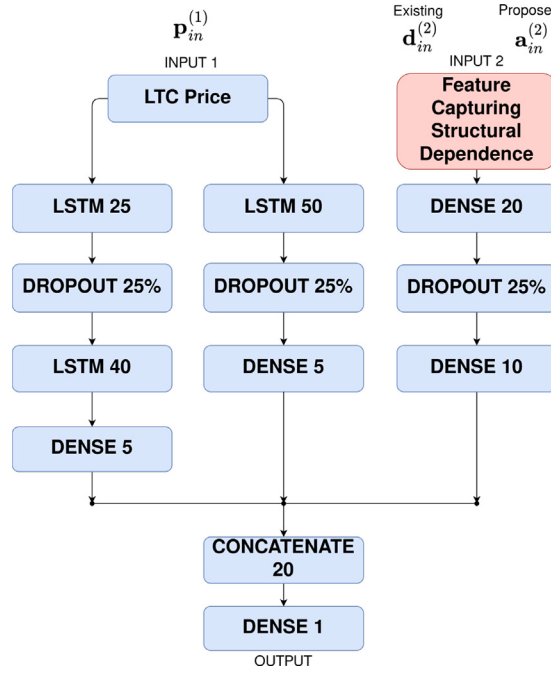


Fig. 29. LSTM based price prediction of LTC — The existing model (Tanwar et al., 2021) uses the BTC price direction, $\mathbf{d}_{in}^{(2)}(i)$, as the input 2, the feature capturing structural dependence. The proposed approach substitutes the input 2 in the existing approach with the BTC component of the posterior mean of mean attractor, $\mathbf{a}_{in}^{(2)}(i)$, for better error performance.

sampled every 5 min from 1 June 2020 to 31 May 2021. All training parameters were kept constant except for input. For input 1, the daily closing prices of LTC were calculated. We computed the BTC component of the posterior mean of the mean attractor of each one day window (considering BTC and LTC), and the BTC price direction, for input 2 of proposed and existing approaches, respectively. To perform LSTM regression, we used 5 time lags (the previous 5 prices) of the daily closing prices of LTC as input 1 for both existing and proposed approaches as in (30).

$$\mathbf{p}_{in}^{(1)}(i) = [p_i, p_{i-1}, \dots, p_{i-4}], \quad (30)$$

Whereas, the input 2 were, 5 time lags of the mean attractors and the parent direction of BTC, for proposed and existing approaches, respectively as in (31) and (32).

$$\mathbf{d}_{in}^{(2)}(i) = [\tau_i^{dir}, \tau_{i-1}^{dir}, \dots, \tau_{i-4}^{dir}], \quad (31)$$

and

$$\mathbf{a}_{in}^{(2)}(i) = [\tau_i^{att}, \tau_{i-1}^{att}, \dots, \tau_{i-4}^{att}]. \quad (32)$$

The corresponding output in both the approaches is,

$$\mathbf{o}(i) = [p_{i+1}]. \quad (33)$$

In (30) through (33), $i = 5, \dots, N - 1$, where N is the total number of training samples.

For the existing approach, the model was trained using the input, $[\mathbf{p}_{in}^1(i), \mathbf{d}_{in}^2(i)]$, and, output $\mathbf{o}(i)$, where $i = 5, \dots, N - 1$. Similarly, for the proposed approach, the model was trained using the input $[\mathbf{p}_{in}^1(i), \mathbf{a}_{in}^2(i)]$, and, output $\mathbf{o}(i)$, where $i = 5, \dots, N - 1$. The estimated price of day $N + 1$, namely \hat{p}_{N+1} , were predicted using the respective trained models, with $[\mathbf{p}_{in}^1(N), \mathbf{d}_{in}^2(N)]$ and $[\mathbf{p}_{in}^1(N), \mathbf{a}_{in}^2(N)]$, as the test inputs for the existing and proposed approaches, respectively. Further, we obtained $\hat{\mathbf{p}}_{in}^1(N + 1) = [\hat{p}_{N+1}, p_N, p_{N-1}, p_{N-2}, p_{N-3}]$, the estimate of $\mathbf{p}_{in}^1(N + 1)$, making use of the latest prediction, \hat{p}_{N+1} . Subsequently, \hat{p}_{N+2} , the estimate of p_{N+2} were obtained using $\hat{\mathbf{p}}_{in}^1(N + 1)$ as test input 1 to the respective models. This process was repeated to obtain predictions over time horizons, up to 14 days.

The performance metric, MSE and MAE over T day prediction is computed as in (34) and (35) respectively.

$$MSE = \frac{1}{T} \sum_{i=N+1}^{N+T} (p_i - \hat{p}_i)^2, \quad T = 1, 2, \dots, 24. \quad (34)$$

$$MAE = \frac{1}{T} \sum_{i=N+1}^{N+T} |p_i - \hat{p}_i|, \quad T = 1, 2, \dots, 24 \quad (35)$$

In order to compare the prediction performances in terms of MSE and MAE, we predicted LTC prices up to a time horizon of 24 days for various values of N , ranging from 90 to 340, using a batch size of 10, over 1000 epochs, and the MSE and MAE values were observed for all iterations. The comparison of MSE and MAE performances up to a time horizon of 14 days are given in Tables 8 and 9, respectively. It can be observed from the Table 8 that the mean MSE of 1 day prediction of the existing method is 0.07, however, it has reduced by almost 28% when the mean attractor is used as one of the input attributes, to 0.05. It can also be observed from the Table 8 that, the mean attractor based approach consistently performs better in terms of mean MSE over all the time horizons of predictions, till 12 days. The mean MSE of 12 day prediction of the proposed approach is 25% better compared to the existing approach. A better MSE performance of the proposed approach signifies that the use of mean attractor as one of the input features, improves the ability of the predictive model to capture extreme events in LTC price variations. However, after 12 days, the average MSE of the proposed method degrades due to the accumulation of uncertainty contributed by the Gaussian Process used to estimate the mean attractor, resulting in a significant number of extreme outliers. However, the MSE performance of the proposed approach, up to the 75th percentile remains consistently better (on an average by 55%) for all prediction horizons, both above and below the 12-day mark, when compared to the existing method. The detailed numerical results of MSE and MAE performances of prediction, up to a time horizon of 24 days, are included in Appendix B.

The MAE performance comparison of both existing and the proposed approaches is given in Table 9. As can be seen from the numerical results, the proposed approach performs consistently better in terms of average MAE, for all the time horizons of predictions, despite the significantly extreme outliers, attributed by the uncertainty propagation. This implies that the use of mean attractor as one of the input attributes have improved the average performance of the LSTM based predictive model.

Table 9

LSTM based price prediction — MAE performance comparison.

	1 Day	2 Day	3 Day	5 Day	7 Day	10 Day	12 Day	13 Day	14 Day
Mean Existing	0.198	0.204	0.209	0.219	0.253	0.284	0.311	0.322	0.333
STD Existing	0.183	0.190	0.196	0.211	0.238	0.260	0.273	0.278	0.283
Mean Proposed	0.176	0.182	0.188	0.197	0.210	0.231	0.244	0.254	0.267
STD Proposed	0.168	0.173	0.182	0.196	0.216	0.284	0.259	0.288	0.313

4.7. Evaluation of the attractor as a feature for price forecasting: An ablation study

In Section 4.6, we presented an LSTM model, which integrated structural dependencies and market indicator features alongside historical cryptocurrency prices for forecasting purposes. In this section, we extend the scope of our analysis to include several other machine learning and deep learning models that are frequently employed in the literature for cryptocurrency price prediction. This evaluation also serves as an ablation study, wherein the impact of incorporating the mean attractor is examined. The observed performance enhancements when the mean attractor is included underscore its importance as a significant feature for price and emphasize its effectiveness as a market indicator.

The models considered in this study are as follows: (i) Artificial Neural Network (ANN) (Miura, Pichl, & Kaizoji, 2019), (ii) Bidirectional Long Short-Term Memory (BiLSTM) (Otabek & Choi, 2024; Seabe, Moutsinga, & Pindza, 2023), (iii) Gated Recurrent Unit (GRU) (Miura et al., 2019; Seabe et al., 2023), (iv) Long Short-Term Memory (LSTM) (Miura et al., 2019; Seabe et al., 2023; Wu, Guo, Fang, & Zhang, 2022), (v) Recurrent Neural Network (RNN) (Miura et al., 2019; Wu et al., 2022), (vi) Support Vector Regression (SVR) (Miura et al., 2019; Wu et al., 2022), and (vii) XGBoost (Wu et al., 2022).

The detailed architectures of these models are provided in the supplementary material. The dataset, along with the training and testing configuration from Section 4.6, which involved training a supervised ML/DL model to predict the price of LTC based on historical prices and structural dependence/market trend data, is applied to the aforementioned models. Specifically, we evaluate these models with five time lags of the historical price of LTC, and five time lags of one of the following structural dependence feature: (i) No additional features, (ii) Mean Bitcoin (BTC) price, (iii) Mean direction of BTC as outlined in Section 4.6, and (iv) Proposed Mean attractor of BTC.

The average Mean Absolute Error (MAE) and Mean Squared Error (MSE) over a 24-day prediction period are presented¹⁰ in Table 10. The MSE and MAE while using the proposed mean attractor is consistently better compared to BTC mean price and mean direction, the existing features used in literature. These findings indicate that the mean attractor proposed in this study is a more effective indicator of the cryptocurrency market for price prediction.

5. Conclusion

Identifying the structural dependence, volatility, and the trends of future price corrections are fundamental to cryptocurrency trading. Owing to extreme volatility in cryptocurrency prices, characterizing the market dynamics, and inferring meaningful features that can capture the price correction trends and structural dependence, based on historic price information is challenging, and it in turn affects, the performance of state-of-the-art machine learning models used in algorithmic trading applications. This paper used a Bayesian Machine Learning technique, namely, Gaussian Process, and the Potential Field theory to develop a unified framework that can simultaneously characterize and quantify:

(a) trends in price movement of cryptocurrencies, (b) structural dependencies between various cryptocurrencies, and (c) volatility. Using the proposed potential field approach, we have analysed the cryptocurrency market data during different BTC crash durations and (i) inferred mean attractors and characterized the volatility, and, uncertainty in price corrections of the cryptocurrencies, (ii) characterized the structural dependencies between various cryptocurrencies, (iii) inferred the direction of asset movement between various cryptocurrencies, (iv) analysed the temporal evolution of attractors and convergence characteristics of the cryptocurrency market, and (v) visualized the structural dependencies, price correction trends and associated uncertainties with the help of self-explanatory diagrams.

A comparison with the wavelet coherence based approach showed that the structural dependency information inferred by the proposed potential field based approach is consistent with the results of popular wavelet coherence approach, while generalizing the approach to more than 2 cryptocurrencies. Further, the inferred mean attractor, when used as an additional input feature in ML/DL based cryptocurrency price forecasting models, on an average, gave 25% better MSE and MAE performance compared to the existing techniques, in predicting the future price of cryptocurrencies.

CRediT authorship contribution statement

Anoop C.V.: Methodology, Conceptualization, Formal analysis, Software, Validation, Investigation, Writing – original draft, Visualization. **Neeraj Negi:** Formal analysis, Data curation, Software, Investigation. **Anup Aprem:** Conceptualization, Supervision, Project administration, Funding acquisition, Writing – review & editing, Resources.

Declaration of competing interest

The authors declare that they have no known competing financial interests or personal relationships that could have appeared to influence the work reported in this paper.

Data availability

Data will be made available on request.

Acknowledgement

This work was supported by a Faculty Research Grant (NIT Calicut) and the Department of Science and Technology FIST Scheme under the Grant SR/FST/ET-I/2017/68.

Appendix A. Recurrence quantification analysis

Recurrence Quantification Analysis (RQA), a tool in chaos theory, used to analyse the observations associated with a nonlinear dynamic system to obtain insights into the predictability, volatility, and informativeness of a dynamic system based on its trajectory. Given a trajectory, $\zeta_{1:N}$, the recurrence matrix, $\mathbf{R} \in \{0, 1\}^{N \times N}$ can be computed as follows:

$$(\mathbf{R})_{i,j} = \begin{cases} 1 & \text{if } \|\mathbf{x}_i - \mathbf{x}_j\|_2 \leq \epsilon \\ 0 & \text{otherwise,} \end{cases} \quad (\text{A.1})$$

¹⁰ Detailed MAE and MSE prediction results for multiple time horizons are included in the appendix.

Table 10

Effectiveness of mean attractor as market indicator: MSE and MAE performance of Ablation study involving various ML/DL models.

Model	Additional feature used	Mean MAE of LTC price prediction (24 Days)	Mean MSE of LTC price prediction (24 Days)
ANN	None	0.63	8.2
	BTC Mean	0.29	0.17
	BTC Mean Direction	0.47	0.6
	BTC Mean Attractor	0.26	0.12
BiLSTM	None	0.38	0.37
	BTC Mean	0.32	0.24
	BTC Mean Direction	0.38	0.47
	BTC Mean Attractor	0.3	0.22
GRU	None	0.39	0.37
	BTC Mean	0.3	0.19
	BTC Mean Direction	0.34	0.26
	BTC Mean Attractor	0.29	0.19
LSTM	None	0.48	0.88
	BTC Mean	0.36	0.43
	BTC Mean Direction	0.35	0.34
	BTC Mean Attractor	0.31	0.26
RNN	None	0.37	0.3
	BTC Mean	0.31	0.23
	BTC Mean Direction	0.34	0.26
	BTC Mean Attractor	0.27	0.16
SVR	None	0.37	0.27
	BTC Mean	0.46	0.59
	BTC Mean Direction	0.43	0.37
	BTC Mean Attractor	0.35	0.26
XGBoost	None	0.35	0.22
	BTC Mean	0.46	0.22
	BTC Mean Direction	0.43	0.23
	BTC Mean Attractor	0.3	0.22

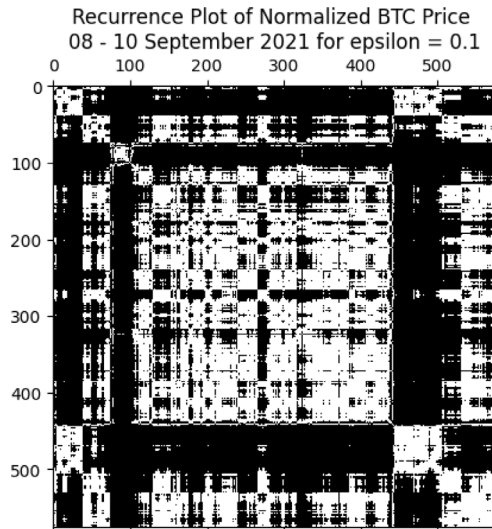


Fig. S.1. Recurrence Plot of Normalized BTC Price. 08–10 September 2021 for $\epsilon = 0.1$.

where, ϵ is a small positive quantity and i and j are row and column indices, respectively of the matrix R . The recurrence matrix as shown in Fig. S.1 reflects the degree to which the states in the trajectory repeats itself over time. The black and white pixels of Fig. S.1 correspond to 0 and 1 respectively. The recurrence matrix is a symmetric matrix, with all the diagonal elements as 1, and hence only the upper or lower diagonal part of the matrix needs to be considered for the analysis. A line in recurrence matrix is referred to as consecutive ones along the rows or columns or along the sub-diagonals.

Fig. S.2 plots the RQA parameters, obtained using the recurrence matrix in (A.1). The various RQA parameters, for the same 72-hour

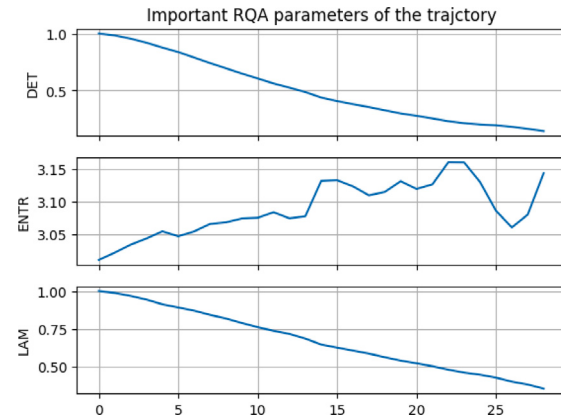


Fig. S.2. Important RQA parameters based on the observations of Bitcoin crash duration. The horizontal axis represents the prediction horizon, in terms of number of samples.

observation period, as in the recurrence plot in Fig. S.1 are defined below: (i) Determinism (DET) measures the proportion of recurrences in the recurrence matrix that are part of a deterministic trajectory. In other words, it quantifies the extent to which the system exhibits repeated patterns of behaviour. DET is calculated as follows:

$$\text{DET} = \frac{\text{sum of diagonal line lengths}}{\text{sum of all line lengths}},$$

where a diagonal line is a continuous sequence of 1's along all the sub diagonals of the recurrence matrix in Fig. S.1. (ii) Entropy (ENTR) measures the degree of randomness or unpredictability in the recurrence matrix. It is calculated as the Shannon entropy of the distribution of diagonal line lengths in Fig. S.1. The Shannon entropy is defined as:

$$\text{ENTR} = - \sum_{\forall i} (p(i) * \log_2(p(i))),$$

Table S.1

LSTM based price prediction — MSE performance of existing approach.

	1 Day	2 Day	3 Day	5 Day	7 Day	10 Day	12 Day	13 Day	14 Day	21 Day	24 Day
mean	0.073	0.081	0.089	0.106	0.139	0.173	0.201	0.213	0.225	0.338	0.409
std	0.147	0.179	0.207	0.27	0.355	0.435	0.471	0.487	0.499	0.624	0.786
min	0.000002	0.00014	0.0002	0.0008	0.0023	0.0035	0.0034	0.0032	0.0031	0.0062	0.007
25%	0.0041	0.0056	0.0070	0.0105	0.0139	0.0190	0.0234	0.0284	0.0303	0.0640	0.0815
50%	0.0208	0.0242	0.0278	0.0323	0.043	0.0648	0.0753	0.0854	0.0914	0.1655	0.1921
75%	0.0858	0.0804	0.0874	0.0976	0.132	0.1632	0.1830	0.1973	0.2114	0.3045	0.3603
max	1.37	1.83	1.99	2.31	2.84	3.57	3.85	4.03	4.08	4.29	5.97

Table S.2

LSTM based price prediction — MSE performance of proposed approach.

	1 Day	2 Day	3 Day	5 Day	7 Day	10 Day	12 Day	13 Day	14 Day	21 Day	24 Day
mean	0.059	0.067	0.074	0.090	0.107	0.143	0.159	0.224	0.266	2.248	15.879
std	0.139	0.17	0.202	0.266	0.347	0.486	0.53	1.259	1.791	32.177	247.163
min	0	0.00004	0.0005	0.0011	0.0020	0.0035	0.0050	0.0048	0.0049	0.0084	0.00780
25%	0.0041	0.0065	0.0079	0.0107	0.0132	0.0194	0.0222	0.0244	0.0253	0.0407	0.0438
50%	0.0163	0.0190	0.0229	0.0271	0.0346	0.0416	0.0447	0.0456	0.0482	0.0749	0.0896
75%	0.061	0.0571	0.063	0.0702	0.0671	0.0802	0.0935	0.0985	0.1026	0.1399	0.1663
max	1.387	1.773	1.922	2.261	2.971	3.82	4.143	18.54	27.37	508.9	3908.22

Table S.3

LSTM based price prediction — MAE performance of existing approach.

	1 Day	2 Day	3 Day	5 Day	7 Day	10 Day	12 Day	13 Day	14 Day	21 Day	24 Day
mean	0.198	0.204	0.209	0.219	0.253	0.284	0.311	0.322	0.333	0.419	0.458
std	0.1837	0.1903	0.196	0.211	0.238	0.260	0.2734	0.2781	0.2833	0.3182	0.344
min	0.0013	0.0109	0.014	0.0244	0.0420	0.0498	0.0473	0.0469	0.0461	0.0640	0.0696
25%	0.0644	0.0661	0.0763	0.0875	0.0968	0.1155	0.1293	0.1352	0.1484	0.2122	0.2437
50%	0.1442	0.1475	0.1507	0.1539	0.1871	0.2190	0.2355	0.2503	0.2551	0.3473	0.3852
75%	0.2928	0.2770	0.2802	0.291	0.3255	0.3650	0.4010	0.4150	0.4329	0.5078	0.5338
max	1.1704	1.3165	1.3857	1.4832	1.6399	1.7905	1.872	1.9203	1.9383	2.0013	2.1484

Table S.4

LSTM based price prediction — MAE performance of proposed approach.

	1 Day	2 Day	3 Day	5 Day	7 Day	10 Day	12 Day	13 Day	14 Day	21 Day	24 Day
mean	0.176	0.182	0.188	0.197	0.210	0.231	0.244	0.254	0.267	0.344	0.435
std	0.1685	0.1739	0.1820	0.1965	0.216	0.2843	0.2599	0.2880	0.3138	0.7783	1.8485
min	0.00017	0.00563	0.018	0.0273	0.0363	0.0532	0.0593	0.0573	0.0578	0.0754	0.0727
25%	0.0644	0.0739	0.0771	0.0873	0.098	0.1172	0.124	0.1282	0.1376	0.1595	0.1698
50%	0.1277	0.1346	0.1401	0.1450	0.1627	0.1752	0.1814	0.1847	0.1843	0.2345	0.2502
75%	0.2474	0.2350	0.2372	0.240	0.229	0.2434	0.2616	0.2704	0.2739	0.3285	0.3498
max	1.1776	1.2953	1.3604	1.4689	1.5421	1.8229	1.9104	2.4474	3.1224	11.7602	29.151

where, $p(i)$ is the probability of a line of length i occurring in the recurrence matrix. (iii) Laminarity (LAM) measures the proportion of recurrences in the recurrence matrix that form vertical or horizontal lines. It quantifies the degree to which the system exhibits periods of stability or laminar behaviour. LAM is calculated as follows:

$$\text{LAM} = \frac{\text{total sum of lengths of vertical and horizontal lines}}{\text{sum of all line lengths}},$$

where, a vertical (or horizontal) line is a continuous sequence of 1's in a column (or row) of the recurrence matrix.

These measures can provide insights into the underlying dynamics of a system and help to characterize its behaviour over time.

In Fig. S.2, the sharp decrease in DET and LAM with increase in prediction horizon¹¹ indicates a very low reliability in future predictions, very poor correlation between nearby states in the trajectory. Similarly, significantly high ENTR across all prediction horizons indicates the highly volatile nature of the cryptocurrency market. The results obtained from RQA analysis emphasize that the system is highly volatile, and any inference about the system should include uncertainty quantification.

Appendix B. LSTM based price prediction of LTC - detailed numerical results

Detailed tabulation of error performances of both the existing and the proposed LSTM based price prediction techniques, up to a prediction horizon of 24 days, are included in this section. The comparison of existing and proposed approaches in terms of mean and standard deviation of both MSE and MAE up to 12 day predictive horizon alone is included in the main document. Though the mean MSE of the proposed predictive approach is deteriorating from day 13 onwards, due to the extreme outliers as a result of the accumulation of uncertainty contributed by the Gaussian Process used to estimate the mean attractor, the MSE performance of the proposed approach, up to the 75th percentile remains consistently better (on an average by 55%) for all prediction horizons, both above and below the 12-day mark, when compared to the existing method (Tables S.1 and S.2). Further, it can also be observed from Tables S.3 and S.4 that, despite extreme outliers, the mean MAE performance of the proposed approach is consistently better throughout all the prediction horizon, compared to the existing method. However, the extremely high outliers, beyond the predictive horizon of day 12, aggravates the uncertainty of the predictive performance of the proposed approach.

¹¹ Time range in which future system outputs are predicted.

Table S.5

Detailed MAE results of Ablation study — up to time horizon of day 24.

Model	Additional Feature	Day 1	Day 3	Day 5	Day 7	Day 10	Day 12	Day 13	Day 14	Day 21	Day 24
ANN	None	0.11	0.16	0.28	0.37	0.51	0.58	0.60	0.66	1.02	1.35
	Mean	0.10	0.15	0.23	0.26	0.29	0.30	0.31	0.32	0.38	0.40
	Mean Dir	0.13	0.17	0.24	0.31	0.40	0.46	0.47	0.51	0.72	0.84
	Attractor	0.10	0.15	0.20	0.23	0.25	0.26	0.27	0.28	0.33	0.36
BiLSTM	None	0.11	0.14	0.24	0.30	0.35	0.39	0.40	0.43	0.52	0.60
	Mean	0.13	0.17	0.23	0.26	0.29	0.32	0.33	0.36	0.44	0.46
	Mean Dir	0.12	0.15	0.21	0.27	0.34	0.38	0.39	0.43	0.56	0.61
	Attractor	0.09	0.14	0.18	0.21	0.26	0.30	0.31	0.34	0.43	0.45
GRU	None	0.12	0.14	0.21	0.28	0.36	0.40	0.41	0.44	0.57	0.63
	Mean	0.12	0.14	0.18	0.22	0.26	0.29	0.30	0.33	0.44	0.45
	Mean Dir	0.12	0.15	0.20	0.25	0.31	0.34	0.35	0.38	0.47	0.51
	Attractor	0.09	0.14	0.17	0.21	0.25	0.28	0.29	0.31	0.41	0.42
LSTM	None	0.12	0.14	0.21	0.28	0.41	0.48	0.50	0.55	0.75	0.85
	Mean	0.13	0.16	0.22	0.26	0.33	0.36	0.37	0.40	0.51	0.53
	Mean Dir	0.12	0.15	0.20	0.26	0.31	0.35	0.36	0.39	0.50	0.54
	Attractor	0.10	0.14	0.18	0.22	0.28	0.31	0.32	0.34	0.44	0.46
RNN	None	0.08	0.12	0.19	0.25	0.34	0.38	0.40	0.43	0.54	0.58
	Mean	0.08	0.13	0.19	0.22	0.28	0.30	0.31	0.33	0.44	0.50
	Mean Dir	0.09	0.13	0.20	0.26	0.33	0.36	0.37	0.39	0.48	0.54
	Attractor	0.07	0.11	0.16	0.19	0.24	0.26	0.27	0.29	0.39	0.46
SVR	None	0.09	0.14	0.24	0.31	0.35	0.36	0.37	0.41	0.51	0.54
	Mean	0.09	0.18	0.32	0.41	0.45	0.49	0.50	0.54	0.61	0.64
	Mean Dir	0.12	0.17	0.27	0.35	0.41	0.45	0.45	0.48	0.58	0.60
	Attractor	0.08	0.13	0.22	0.27	0.33	0.36	0.37	0.39	0.50	0.53
XGBoost	None	0.09	0.13	0.22	0.27	0.33	0.36	0.37	0.39	0.50	0.54
	Mean	0.09	0.18	0.32	0.41	0.45	0.49	0.50	0.54	0.61	0.64
	Mean Dir	0.12	0.17	0.27	0.35	0.41	0.45	0.45	0.48	0.58	0.60
	Attractor	0.08	0.13	0.19	0.23	0.28	0.30	0.31	0.32	0.43	0.48

Table S.6

Detailed MSE results of Ablation study — up to time horizon of day 24.

Model	Additional Feature	Day 1	Day 3	Day 5	Day 7	Day 10	Day 12	Day 13	Day 14	Day 21	Day 24
ANN	None	0.020	0.053	0.147	0.264	0.555	0.892	1.042	1.612	1.719	1.912
	Mean	0.019	0.044	0.094	0.131	0.159	0.176	0.179	0.186	0.257	0.311
	Mean Dir	0.030	0.057	0.122	0.194	0.298	0.362	0.383	0.451	1.177	2.485
	Attractor	0.018	0.038	0.072	0.091	0.108	0.117	0.120	0.129	0.179	0.214
BiLSTM	None	0.021	0.127	0.365	0.341	0.252	0.312	0.329	0.371	0.504	0.882
	Mean	0.040	0.076	0.131	0.151	0.182	0.233	0.249	0.292	0.388	0.397
	Mean Dir	0.030	0.053	0.121	0.225	0.372	0.457	0.482	0.552	0.825	0.928
	Attractor	0.016	0.034	0.062	0.089	0.140	0.191	0.210	0.262	0.388	0.403
GRU	None	0.026	0.038	0.104	0.191	0.310	0.347	0.359	0.394	0.642	0.761
	Mean	0.027	0.036	0.063	0.093	0.131	0.160	0.170	0.203	0.355	0.357
	Mean Dir	0.029	0.048	0.097	0.155	0.216	0.262	0.274	0.303	0.446	0.527
	Attractor	0.016	0.034	0.059	0.086	0.135	0.171	0.181	0.212	0.335	0.348
LSTM	None	0.024	0.044	0.108	0.207	0.649	0.970	1.018	1.133	1.638	1.979
	Mean	0.030	0.052	0.128	0.237	0.375	0.453	0.477	0.542	0.701	0.730
	Mean Dir	0.029	0.047	0.105	0.188	0.284	0.346	0.363	0.404	0.583	0.676
	Attractor	0.021	0.035	0.069	0.115	0.202	0.259	0.275	0.319	0.444	0.471
RNN	None	0.014	0.034	0.087	0.145	0.240	0.292	0.308	0.355	0.533	0.626
	Mean	0.014	0.035	0.084	0.133	0.196	0.221	0.227	0.245	0.400	0.507
	Mean Dir	0.016	0.039	0.094	0.147	0.219	0.254	0.263	0.289	0.445	0.543
	Attractor	0.010	0.024	0.052	0.081	0.126	0.141	0.148	0.171	0.283	0.384
SVR	None	0.015	0.046	0.117	0.171	0.235	0.269	0.277	0.301	0.455	0.527
	Mean	0.019	0.101	0.350	0.526	0.551	0.604	0.623	0.674	0.849	0.969
	Mean Dir	0.026	0.066	0.155	0.248	0.336	0.390	0.402	0.439	0.590	0.679
	Attractor	0.014	0.039	0.104	0.170	0.213	0.232	0.246	0.286	0.426	0.463
XGBoost	None	0.019	0.042	0.096	0.144	0.191	0.206	0.212	0.232	0.367	0.469
	Mean	0.020	0.043	0.092	0.135	0.181	0.197	0.204	0.224	0.370	0.469
	Mean Dir	0.019	0.045	0.100	0.150	0.196	0.213	0.221	0.246	0.382	0.483
	Attractor	0.018	0.041	0.092	0.134	0.181	0.200	0.205	0.223	0.367	0.466

Appendix C. Ablation study: Detailed numerical results

The Mean Squared Error and Mean Absolute Error performance was computed for various machine learning models for prediction horizon ranging from 1 to 24 days. The details of MAE and MSE for different prediction horizon are included in Tables S.5 and S.6, respectively.

As can be seen from Tables S.5 and S.6, including the attractor consistently outperforms using the mean Bitcoin value or direction, the existing approach in cryptocurrency price prediction. The performance improvements observed provide strong evidence of its importance as a feature and validate its effectiveness as a market indicator. The architecture of the ML and DL models utilized in Section 4.7 is provided in the supplementary material.

Appendix D. Supplementary data

Supplementary material related to this article can be found online at <https://doi.org/10.1016/j.eswa.2024.125475>.

References

- Abraham, J., Higdon, D., Nelson, J., & Ibarra, J. (2018). Cryptocurrency price prediction using tweet volumes and sentiment analysis. *SMU Data Science Review*, 1(3), 1–21.
- Akyildirim, E., Goncu, A., & Sensoy, A. (2021). Prediction of cryptocurrency returns using machine learning. *Annals of Operations Research*, 297, 3–36.
- Alatorre, D., Gershenson, C., & Mateos, J. L. (2023). Stocks and cryptocurrencies: Antifragile or robust? A novel antifragility measure of the stock and cryptocurrency markets. *Plos One*, 18(3), Article e0280487.
- Almeida, D., Dionísio, A., Vieira, I., & Ferreira, P. (2023). COVID-19 effects on the relationship between cryptocurrencies: Can it be contagion? Insights from econophysics approaches. *Entropy*, 25(1), 98–105.
- Antonakakis, N., Chatziantoniou, I., & Gabauer, D. (2019). Cryptocurrency market contagion: Market uncertainty, market complexity, and dynamic portfolios. *Journal of International Financial Markets, Institutions and Money*, 61, 37–51.
- Aras, S. (2021). Stacking hybrid GARCH models for forecasting bitcoin volatility. *Expert Systems with Applications*, 174, Article 114747.
- Balcioğlu, Y. S., & Özer, G. (2023). What proportion of the bitcoin ecosystem is controlled by bots? In *Global economic challenges: 6th intrn. conf. on banking and finance perspectives* (pp. 31–38). Springer.
- Berkenkamp, F., Schoellig, A. P., & Krause, A. (2019). No-regret Bayesian optimization with unknown hyperparameters. *Journal of Machine Learning Research*, 20(50), 1–24.
- Biswal, B., & Dasgupta, C. (2002). Stochastic neural network model for spontaneous bursting in hippocampal slices. *Physical Review E*, 66(5), Article 051908-1–051908-18.
- Cambel, A. B. (1993). *Applied chaos theory: A paradigm for complexity*. Elsevier.
- Chai, T., & Draxler, R. R. (2014). Root mean square error (RMSE) or mean absolute error (MAE). *Geoscientific Model Development Discussions*, 7(1), 1525–1534.
- Cheah, E.-T., & Fry, J. (2015). Speculative bubbles in bitcoin markets? An empirical investigation into the fundamental value of bitcoin. *Economics Letters*, 130, 32–36.
- Chuen, D. L. K., Guo, L., & Wang, Y. (2017). Cryptocurrency: A new investment opportunity? *The Journal of Alternative Investments*, 20(3), 16–40.
- Cobb, A. D., Everett, R., Markham, A., & Roberts, S. J. (2018). Identifying sources and sinks in the presence of multiple agents with gaussian process vector calculus. In *Proc. of the 24th ACM SIGKDD intrn. conf. on knowledge discovery & data mining* (pp. 1254–1262).
- Critten, J. V., Gatt, A., & Ellul, J. (2022). Bitcoin price change and trend prediction through twitter sentiment and data volume. *Financial Innovation*, 8(1), 1–20.
- de Miranda Cardoso, J. V., Ying, J., & Palomar, D. (2021). Graphical models in heavy-tailed markets. In *Advances in neural information processing systems: vol. 34*, (pp. 19989–20001).
- Fang, F., Ventre, C., Basios, M., Kanthan, L., Martinez-Rego, D., Wu, F., et al. (2022). Cryptocurrency trading: A comprehensive survey. *Financial Innovation*, 8(1), 1–59.
- Fei, Y., Shi, P., & Lim, C.-C. (2023). Robust and collision-free formation control of multiagent systems with limited information. *IEEE Transactions on Neural Networks and Learning Systems*, 34(8), 4286–4295. <http://dx.doi.org/10.1109/TNNLS.2021.3112679>.
- Fruehwirth, W., Hochfilzer, L., Weydemann, L., & Roberts, S. (2021). Cumulation, crash, coherency: A cryptocurrency bubble wavelet analysis. *Finance Research Letters*, 40, 101668–101683.
- Gajamannage, K., Park, Y., & Jayathilake, D. I. (2023). Real-time forecasting of time series in financial markets using sequentially trained dual-LSTMs. *Expert Systems with Applications*, 223, Article 119879.
- Gao, Z., He, Y., & Kuruoglu, E. E. (2021). A hybrid model integrating LSTM and GARCH for bitcoin price prediction. In *IEEE 31st intrn. workshop on machine learning for signal processing* (pp. 1–6).
- Hassani, H., Huang, X., & Silva, E. (2018). Big-crypto: Big data, blockchain and cryptocurrency. *Big Data and Cognitive Computing*, 2(4), 34–48.
- Herzen, J., Lässig, F., Piazzetta, S. G., Neuer, T., Tafti, L., Raille, G., et al. (2022). Darts: User-friendly modern machine learning for time series. *Journal of Machine Learning Research*, 23(124), 1–6.
- Ji, S., Pan, S., Cambria, E., Marttinen, P., & Yu, P. S. (2022). A survey on knowledge graphs: Representation, acquisition, and applications. *IEEE Transactions on Neural Networks and Learning Systems*, 33(2), 494–514. <http://dx.doi.org/10.1109/TNNLS.2021.3070843>.
- Jiang, S., Zhou, J., & Qiu, S. (2023). Is there any correlation between digital currency price fluctuation? based on the DCC-GARCH and wavelet coherence analysis. *Economic Research-Ekonomska Istraživanja*, 36(2), 2134901–2134926.
- Jing, L., & Kang, Y. (2024). Automated cryptocurrency trading approach using ensemble deep reinforcement learning: Learn to understand candlesticks. *Expert Systems with Applications*, 237, Article 121373.
- Khedr, A. M., Arif, I., El-Bannany, M., Alhashmi, S. M., & Sreedharan, M. (2021). Cryptocurrency price prediction using traditional statistical and machine-learning techniques: A survey. *Intelligent Systems in Accounting, Finance and Management*, 28(1), 3–34.
- Khosravi, M., & Ghazani, M. M. (2023). Novel insights into the modeling financial time-series through machine learning methods: Evidence from the cryptocurrency market. *Expert Systems with Applications*, 234, Article 121012.
- Khurana, S. S., Singh, P., & Garg, N. K. (2023). Revolutionize AI trading bots with autoML-based multi-timeframe bitcoin price prediction. *SN Computer Science*, 4(5), 492.
- Kumbure, M. M., Lohrmann, C., Luukka, P., & Porras, J. (2022). Machine learning techniques and data for stock market forecasting: A literature review. *Expert Systems with Applications*, 197, Article 116659.
- Kumlungmak, K., & Vateekul, P. (2023). Multi-agent deep reinforcement learning with progressive negative reward for cryptocurrency trading. *IEEE Access*, 66440–66455.
- Lahmiri, S., Bekiros, S., & Bezzina, F. (2022). Complexity analysis and forecasting of variations in cryptocurrency trading volume with support vector regression tuned by Bayesian optimization under different kernels: An empirical comparison from a large dataset. *Expert Systems with Applications*, 209, Article 118349.
- Letham, B., & Bakshy, E. (2019). Bayesian optimization for policy search via online-offline experimentation. *Journal of Machine Learning Research*, 20(145), 1–30.
- Lisa, A. (2021). 7 biggest bitcoin crashes-history. <https://finance.yahoo.com/news/7-biggest-bitcoin-crashes-history-180038282.html>. (Accessed on 1 June 2023).
- Ma, Y., Tan, Q., Yuan, R., Yuan, B., & Ao, P. (2014). Potential function in a continuous dissipative chaotic system: Decomposition scheme and role of strange attractor. *International Journal of Bifurcation and Chaos*, 24(02), Article 1450015.
- Majidi, N., Shamsi, M., & Marvasti, F. (2024). Algorithmic trading using continuous action space deep reinforcement learning. *Expert Systems with Applications*, 235, Article 121245.
- Meng, F., Shi, S., Zhang, B., Bai, M., & Lin, N. (2022). Analysis for global characteristics of Lyapunov exponents in vehicle plane motion system. *Scientific Reports*, 12(1), Article 9300–1–9300–14.
- Miura, R., Pichl, L., & Kaizoji, T. (2019). Artificial neural networks for realized volatility prediction in cryptocurrency time series. In *Advances in neural networks-ISNN 2019: 16th international symposium on neural networks, ISNN 2019, moscow, Russia, July 10–12, 2019, proceedings, Part I* 16 (pp. 165–172). Springer.
- Mudassir, M., Bennbaia, S., Unal, D., & Hammoudeh, M. (2020). Time-series forecasting of bitcoin prices using high-dimensional features: A machine learning approach. *Neural Computing and Applications*, 1–15.
- Murphy, K. P. (2012). *Machine learning: A probabilistic perspective*. MIT Press.
- Murray, K., Rossi, A., Carraro, D., & Visentin, A. (2023). On forecasting cryptocurrency prices: A comparison of machine learning, deep learning, and ensembles. *Forecasting*, 5(1), 196–209.
- Otabek, S., & Choi, J. (2024). From prediction to profit: A comprehensive review of cryptocurrency trading strategies and price forecasting techniques. *IEEE Access*, 12, 87039–87064.
- Parente, M., Rizzuti, L., & Trerotola, M. (2024). A profitable trading algorithm for cryptocurrencies using a neural network model. *Expert Systems with Applications*, 238, Article 121806.
- Peng, P., Chen, Y., Lin, W., & Wang, J. Z. (2024). Attention-based CNN-LSTM for high-frequency multiple cryptocurrency trend prediction. *Expert Systems with Applications*, 237, Article 121520.
- Phillips, R. C., & Gorse, D. (2018). Cryptocurrency price drivers: Wavelet coherence analysis revisited. *PLoS One*, 13(4), 1–21.
- Qiao, X., Zhu, H., & Hau, L. (2020). Time-frequency co-movement of cryptocurrency return and volatility: Evidence from wavelet coherence analysis. *International Review of Financial Analysis*, 71, Article 101541.
- Roberts, S., Osborne, M., Ebden, M., Reece, S., Gibson, N., & Aigrain, S. (2013). Gaussian processes for time-series modelling. *Philosophical Transactions of the Royal Society of London A (Mathematical and Physical Sciences)*, 371(1984), Article 20110550.
- Rosenstein, M. T., Collins, J. J., & De Luca, C. J. (1993). A practical method for calculating largest Lyapunov exponents from small data sets. *Physica D: Nonlinear Phenomena*, 65(1–2), 117–134.
- Rubio Scola, I., Garcia Carrillo, L. R., & Hespanha, J. P. (2023). Limbic system-inspired performance-guaranteed control for nonlinear multi-agent systems with uncertainties. *IEEE Transactions on Neural Networks and Learning Systems*, 34(8), 4196–4207. <http://dx.doi.org/10.1109/TNNLS.2021.3121232>.
- Sanders, H., & Saxe, J. (2017). Garbage in, garbage out: how purportedly great ML models can be screwed up by bad data. In *Proc. of Blackhat*.
- Schulz, E., Speekenbrink, M., & Krause, A. (2018). A tutorial on Gaussian process regression: Modelling, exploring, and exploiting functions. *Journal of Mathematical Psychology*, 85, 1–16.
- Seabe, P. L., Moutsinga, C. R. B., & Pindza, E. (2023). Forecasting cryptocurrency prices using LSTM, GRU, and bi-directional LSTM: A deep learning approach. *Fractal and Fractional*, 7(2).
- Sezer, O., Gudelek, M., & Ozbayoglu, A. (2020). Financial time series forecasting with deep learning: A systematic literature review: 2005–2019. *Applied Soft Computing*, 90, 106181–1061243.
- Shen, Z., Wan, Q., & Leatham, D. J. (2021). Bitcoin return volatility forecasting: A comparative study between GARCH and RNN. *Journal of Risk and Financial Management*, 14(7), 337–354.
- Srinivas Murthy, A., Akshay, A., & Hanji, B. R. (2022). Cryptocurrency trading bot with sentimental analysis and backtracking using predictive ML. In *International conference on innovations in computer science and engineering* (pp. 501–512). Springer.

- Tanwar, S., Patel, N. P., Patel, S. N., Patel, J. R., Sharma, G., & Davidson, I. E. (2021). Deep learning-based cryptocurrency price prediction scheme with inter-dependent relations. *IEEE Access*, 9, 138633–138646.
- Tran, B.-H., Rossi, S., Milios, D., & Filippone, M. (2022). All you need is a good functional prior for Bayesian deep learning. *Journal of Machine Learning Research*, 23(74), 1–56.
- Vassiliadis, S., Papadopoulos, P., Rangoussi, M., Konieczny, T., & Gralewski, J. (2017). Bitcoin value analysis based on cross-correlations. *Journal of Internet Banking and Commerce*, 22(7), 1–12.
- Vulpiani, A., Cecconi, F., & Cencini, M. (2009). *Chaos: from simple models to complex systems: vol. 17*, World Scientific.
- Webber, Jr., C. L., & Zbilut, J. P. (2005). Recurrence quantification analysis of nonlinear dynamical systems. In *Tutorials in contemporary nonlinear methods for the behavioral sciences: vol. 94*, (pp. 26–94).
- Williams, C. K., & Rasmussen, C. E. (2006). *Gaussian processes for machine learning: vol. 2*, (3), Cambridge, MA: MIT Press.
- Willmott, C. J., & Matsuura, K. (2005). Advantages of the mean absolute error (MAE) over the root mean square error (RMSE) in assessing average model performance. *Climate Research*, 30(1), 79–82.
- Wu, J., Guo, X., Fang, M., & Zhang, J. (2022). Short term return prediction of cryptocurrency based on XGBoost algorithm. In *2022 International conference on big data, information and computer network* (pp. 39–42).
- Yuan, R.-S., Ma, Y.-A., Yuan, B., & Ao, P. (2013). Lyapunov function as potential function: A dynamical equivalence. *Chinese Physics B*, 23(1), Article 010505–1–010505–6.
- Zhao, T., Ma, X., Li, X., & Zhang, C. (2023). Asset correlation based deep reinforcement learning for the portfolio selection. *Expert Systems with Applications*, 221, Article 119707.
- Zhong, C., Du, W., Xu, W., Huang, Q., Zhao, Y., & Wang, M. (2023). LSTM-ReGAT: A network-centric approach for cryptocurrency price trend prediction. *Decision Support Systems*, 169, 113955–113964.
- Zhou, Z., Song, Z., Xiao, H., & Ren, T. (2023). Multi-source data driven cryptocurrency price movement prediction and portfolio optimization. *Expert Systems with Applications*, 219, Article 119600.